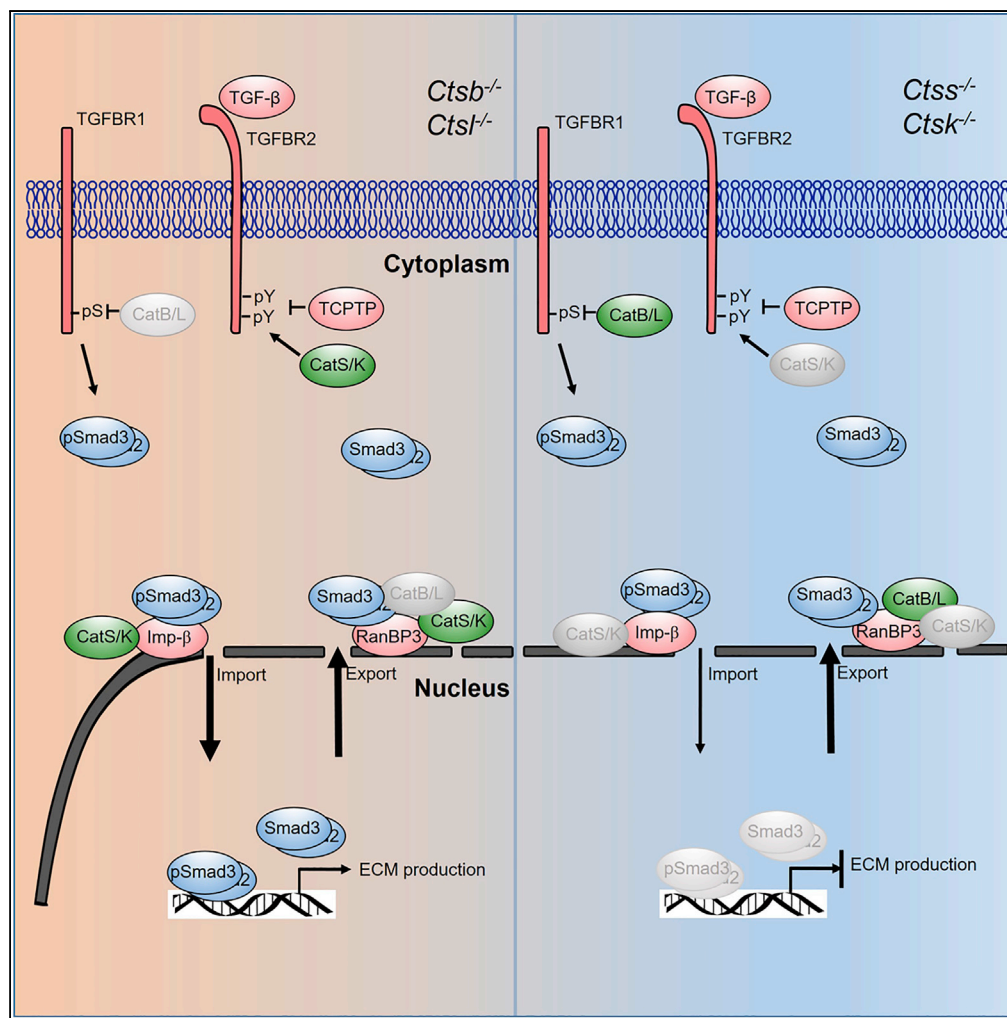


Article

Differential Roles of Cysteinyil Cathepsins in TGF- β Signaling and Tissue Fibrosis



Xian Zhang, Yi Zhou, Xueqing Yu, ..., Galina K. Sukhova, Peter Libby, Guo-Ping Shi

gshi@bwh.harvard.edu

HIGHLIGHTS

Cathepsins exert different activities in kidney TEC TGF- β signaling and fibrosis

Cathepsins regulate nuclear membrane transporter expression and form immunocomplexes

Cathepsins regulate plasma membrane TGF- β receptor expression and form immunocomplexes

Cathepsins play different roles in acute injury-induced kidney fibrosis

Zhang et al., iScience 19, 607–622
 September 27, 2019 © 2019 The Author(s).
<https://doi.org/10.1016/j.isci.2019.08.014>



Article

Differential Roles of Cysteinyln Cathepsins in TGF- β Signaling and Tissue Fibrosis

Xian Zhang,^{1,2,5} Yi Zhou,^{1,3,5} Xueqing Yu,³ Qin Huang,^{1,4} Wenqian Fang,¹ Jie Li,¹ Joseph V. Bonventre,¹ Galina K. Sukhova,¹ Peter Libby,¹ and Guo-Ping Shi^{1,6,*}

SUMMARY

Transforming growth factor beta (TGF- β) signaling contributes to tissue fibrosis. Here we demonstrate that TGF- β enhances CatS and CatK expression but reduces CatB and CatL expression in mouse kidney tubular epithelial cells (TECs). CatS- and CatK deficiency reduces TEC nuclear membrane importer importin- β expression, Smad-2/3 activation, and extracellular matrix (ECM) production. Yet CatB- and CatL-deficiency displays the opposite observations with reduced nuclear membrane exporter RanBP3 expression. CatS and CatK form immunocomplexes with the importin- β and RanBP3 more effectively than do CatB and CatL. On the plasma membrane, CatS and CatK preferentially form immunocomplexes with and activate TGF- β receptor-2, whereas CatB and CatL form immunocomplexes with and inactivate TGF- β receptor-1. Unilateral ureteral obstruction-induced renal injury tests differential cathepsin activities in TGF- β signaling and tissue fibrosis. CatB- or CatL-deficiency exacerbates fibrosis, whereas CatS- or CatK-deficiency protects kidneys from fibrosis. These cathepsins exert different effects in the TGF- β signaling cascade independent of their proteolytic properties.

INTRODUCTION

Transforming growth factor beta (TGF- β), a pleiotropic mediator of fibrotic remodeling, induces myofibroblast transition, Smad activation, and extracellular matrix (ECM) production; inhibits excessive ECM protein degradation by regulation of proteases and their endogenous inhibitors; and regulates integrin expression and cell adhesion to the matrix (Border and Noble, 1994; Lan, 2003). Active TGF- β binds to TGF- β receptor-2 (TGFBR2). This binding recruits and activates TGF- β receptor-1 (TGFBR1) (Massague, 1998), followed by phosphorylation of Smad-2 and Smad-3 (Roberts, 1998; Schnaper et al., 2002). Phosphorylated Smad-2 and Smad-3 (pSmad-2/3) and Smad-4 form a Smad complex (Feng and Derynck, 2005) that translocates to the nucleus to regulate the expression of profibrotic genes such as collagen, fibronectin, and α -smooth muscle actin (α -SMA) (Massague, 1998), leading to tissue fibrosis that characterizes diseases of multiple tissues and organs. Cells denoted myofibroblasts elaborate ECM in response to TGF- β and can arise from fibroblasts, endothelial cells, epithelial cells, or even macrophages (Allison, 2013; LeBleu et al., 2013; Meng et al., 2014; Nikolic-Paterson et al., 2014).

TGF- β signaling and Smad activation determine ECM production and tissue fibrosis. Lungs from patients with cystic fibrosis and idiopathic pulmonary fibrosis (IPF) show increased pSmad-2, the myofibroblast marker α -SMA, and collagen deposition (Harris et al., 2013). Transgenic expression of TGF- β augments macrophage-dependent lung fibrosis (Murray et al., 2011). Lung epithelial cell-specific depletion of TGFBR2 protects mice from bleomycin-induced fibrosis (Li et al., 2011). Elevated TGF- β in infarcted hearts correlates with impaired left ventricular function (Talasaz et al., 2013). Continued TGF- β activation promotes chronic hypertension, progressive myocardial fibrosis, and heart failure. Infarcted hearts from Smad-3-deficient mice show reduced fibrosis (Bujak et al., 2007), and fibroblasts from these mice do not respond to TGF- β (Verrecchia et al., 2001). Chronic liver damage-induced TGF- β activates hepatic stellate cell (HSC)-to-myofibroblast transition and hepatocyte death and promotes liver fibrosis, cirrhosis, and ultimately hepatocellular carcinoma (Dongiovanni et al., 2014). Chronic kidney diseases involve renal fibrosis that contributes to organ failure (Eddy and Neilson, 2006). TGF- β 1 induces tubular epithelial cell (TEC)-to-myofibroblast transition and promotes renal fibrosis (Lan, 2003).

Cysteinyln cathepsins mediate ECM protein degradation and mitigate tissue fibrosis. TGF- β lowers cathepsin L (CatL) expression in lung epithelial cells (Gerber et al., 2001) and cathepsin K (CatK) expression in fibroblasts, favoring lung fibrosis (van den Brule et al., 2005). Deficiency of CatK or CatL exacerbates lung and myocardial fibrosis and cardiomyopathy (Buhling et al., 2004; Petermann et al., 2006), whereas their

¹Department of Medicine, Cardiovascular Medicine, Brigham and Women's Hospital, Harvard Medical School, 77 Avenue Louis Pasteur, NRB-7, Boston, MA 02115, USA

²School of Food & Biological Engineering, Hefei University of Technology, Hefei 230009, China

³Department of Nephrology, First Affiliated Hospital, Sun Yat-Sen University, Guangzhou 510080, China

⁴Department of Rheumatology, Nanfang Hospital, Southern Medical University, Guangzhou 510515, China

⁵These authors contributed equally

⁶Lead Contact

*Correspondence: gshi@bwh.harvard.edu
<https://doi.org/10.1016/j.isci.2019.08.014>



overexpression reduces ECM deposition, cardiac hypertrophy, and cardiac and lung fibrosis (Tang et al., 2009; Zhang et al., 2011a, 2011b). These studies suggest a protective role of cathepsins in tissue fibrosis via their ECM degradation. Yet, fibroblasts in fibrotic lungs from patients with IPF express high levels of CatK. CatK inhibition decreases pSmad-2/3, diminishes α -SMA expression, and delays fibroblast differentiation (Buhling et al., 2004). In bleomycin-induced lung fibrosis, cathepsin activities increase in lung homogenates and in lavage fluid (Kasabova et al., 2016). Liver CatL and cathepsin B (CatB) levels also increase in patients with hepatic cirrhosis and in mice with CCl₄-induced liver fibrosis (Manchanda et al., 2017). CatB inhibition or depletion reduces mouse liver inflammation and fibrogenesis (Moles et al., 2009, 2012). Deficiency of cathepsin S (CatS) reduces mouse myofibroblast differentiation and Smad activation and impairs post-infarct cardiac functions (Chen et al., 2013). Therefore, cathepsin activities beyond ECM degradation may contribute to tissue fibrosis.

This study used kidney TECs from mice deficient in CatB, CatL, CatS, and CatK and demonstrated that individual members of this highly related class of cathepsins contributed in opposing manners to TGF- β signaling, Smad activation, and profibrotic protein production. These distinct activities arose from differential regulation of cathepsin expression and interaction with and activation of nuclear membrane Smad complex transporter proteins (importin- β and RanBP3) and plasma membrane TGF- β receptors (TGFBR2 and TGFBR1). We validated these observations in fibrosis-dependent unilateral ureteral obstruction (UUO)-induced mouse renal injury, in which individual cathepsins showed opposite activities in renal Smad activation, epithelial cell differentiation, and kidney fibrosis.

RESULTS

Differential Role of Cathepsins in TGF- β -Induced ECM Production in Mouse Kidney TECs

TGF- β promotes kidney TECs epithelial-mesenchymal-transition into myofibroblasts that release pro-inflammatory and profibrotic proteins during renal fibrogenesis (Grande et al., 2015; LeBleu et al., 2013; Lovisa et al., 2015). Kidney TECs were isolated from wild-type (WT), *Ctsb*^{-/-}, *Ctsl*^{-/-}, *Ctss*^{-/-}, and *Ctsk*^{-/-} mice and characterized by immunofluorescent staining for the epithelial marker E-cadherin and for the proximal tubule epithelial cell marker aquaporin-1 (Figure S1A). Over 95% of Cultured TECs displayed E-cadherin by flow cytometry analysis (Figure S1B). TGF- β promoted acquisition of a fibrotic phenotype by TECs characterized by reduced E-cadherin expression and increased α -SMA expression (Figure S1C). Immunoblot analysis (Figure 1A) and immunofluorescent staining (Figure 1B) showed that TGF- β increased the expression of CatS and CatK but reduced the expression of CatB and CatL in mouse kidney TECs. To test whether differential expression of these cathepsins affected differently TEC fibrotic phenotype changes or differentiation into myofibroblasts, we treated TECs from cathepsin-deficient mice with TGF- β . Both immunoblot analysis (Figure 1C) and immunofluorescent staining (Figure 1D) showed that deficiency of CatS or CatK reduced the production of α -SMA and fibronectin, whereas deficiency of CatB or CatL increased the expression of these fibrotic proteins in TECs after TGF- β stimulation, as compared with TECs from WT control mice. Therefore, in mouse TECs, TGF- β acted differently in regulating the expression of different cathepsins and different cathepsins also showed varying activities in regulating the expression of TGF- β -induced profibrotic genes.

Differential Activity of Cathepsins in Kidney TEC Smad Activation

TGF- β signaling and Smad activation drive TEC myofibroblast differentiation. Translocation of pSmad-2/3 to the nucleus precedes profibrotic gene transcription and tissue fibrosis (Grande et al., 2015; Lan, 2003; Lovisa et al., 2015; Nikolic-Paterson et al., 2014). Altered profibrotic gene expression in TECs from different cathepsin-deficient mice suggests that these cathepsins exert different activities in Smad activation. Phosphorylation of Smad-2 and Smad-3 peaked at 20 to 40 min (Figure 2A) when TECs from WT mice were treated with TGF- β (2 ng/mL). Under the same conditions (2 ng/mL TGF- β , 20 min), pSmad-2/3 in TECs from CatS- and CatK-deficient mice showed greatly reduced levels, yet displayed highly increased levels in TECs from CatB- and CatL-deficient mice (Figure 2B). Increased pSmad-3 activation in TECs from CatB- and CatL-deficient mice and decreased pSmad-3 activation in TECs from CatS- and CatK-deficient mice occurred in the nuclear fraction, whereas total Smad-3 expression revealed itself in both nuclear and cytoplasmic fractions, as shown by immunoblot analysis. Fibrillarin and β -actin immunoblots validated the separation of nuclear and cytoplasmic fractions (Figure 2C). Consistent with the immunoblot results, after TGF- β stimulation, positive immunofluorescent staining with anti-pSmad-2 (Figure 2D) and anti-pSmad-3 (Figure 2E) antibodies detected increased nuclear pSmad-2/3 in TECs from *Ctsb*^{-/-} and *Ctsl*^{-/-} mice but reduced nuclear pSmad-2/3 in those from *Ctss*^{-/-} and *Ctsk*^{-/-} mice. These observations suggested that

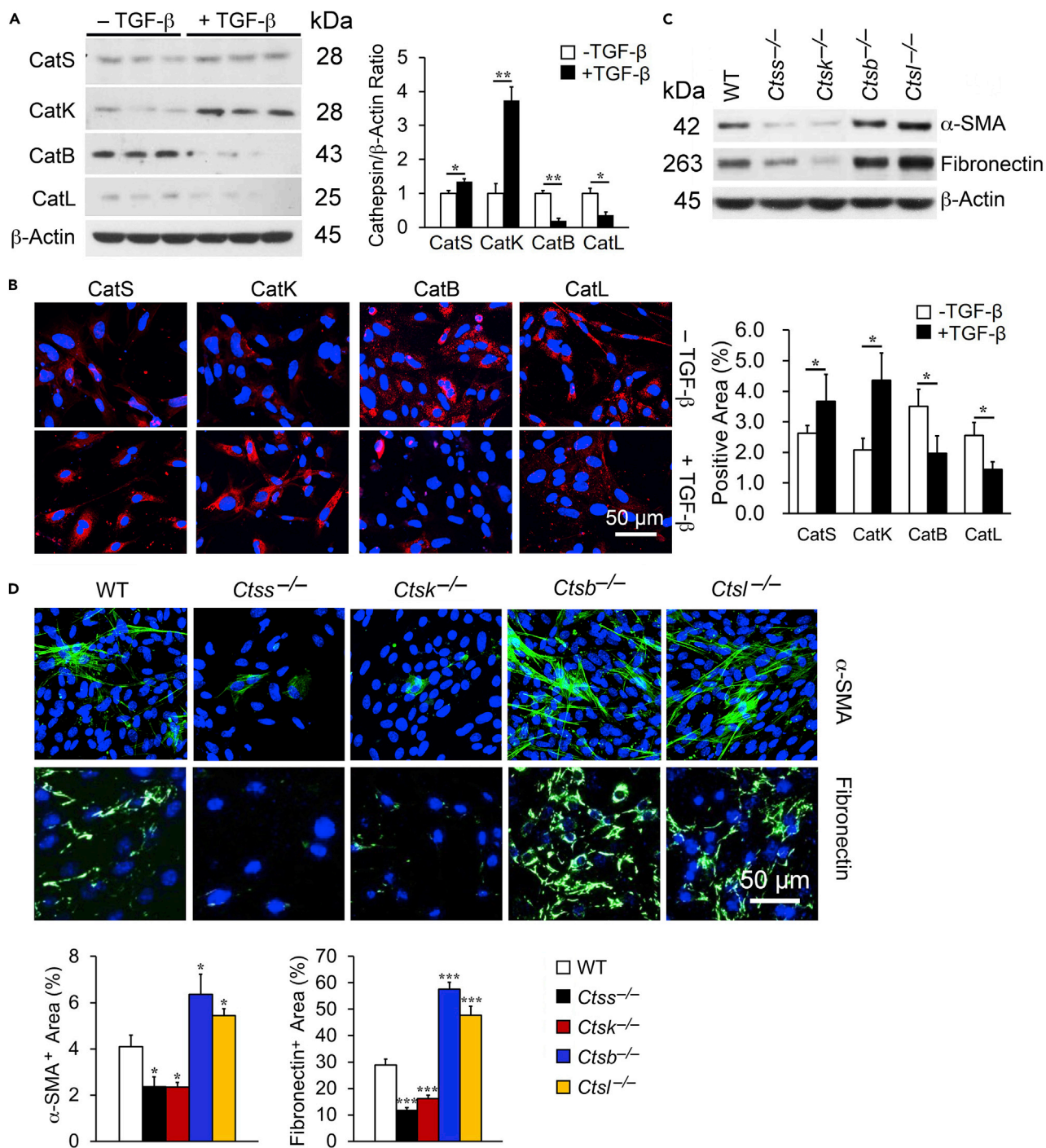


Figure 1. TGF-β-Regulated Expression of Cathepsins and Fibrotic Proteins in Mouse Kidney TECs

(A–D) Immunoblot (A) and immunofluorescent staining detected the expression of CatB, CatL, CatS, and CatK (red) with nuclei counterstained with DAPI (blue) and quantification (B) in WT kidney TECs with or without 2 ng/mL TGF-β stimulation. Immunoblot (C) and immunofluorescent staining detected the expression of α-SMA (green) and fibronectin (green) with nuclei counterstained with DAPI (blue) and quantification (D) in TGF-β-treated (2 ng/mL, 24h) TECs from WT, *Ctsb*^{-/-}, *Ctsl*^{-/-}, *Ctss*^{-/-}, and *Ctsk*^{-/-} mice.

Scale bar: 50 μm. Data are representative of four independent experiments. *p < 0.05, **p < 0.01, ***p < 0.001.

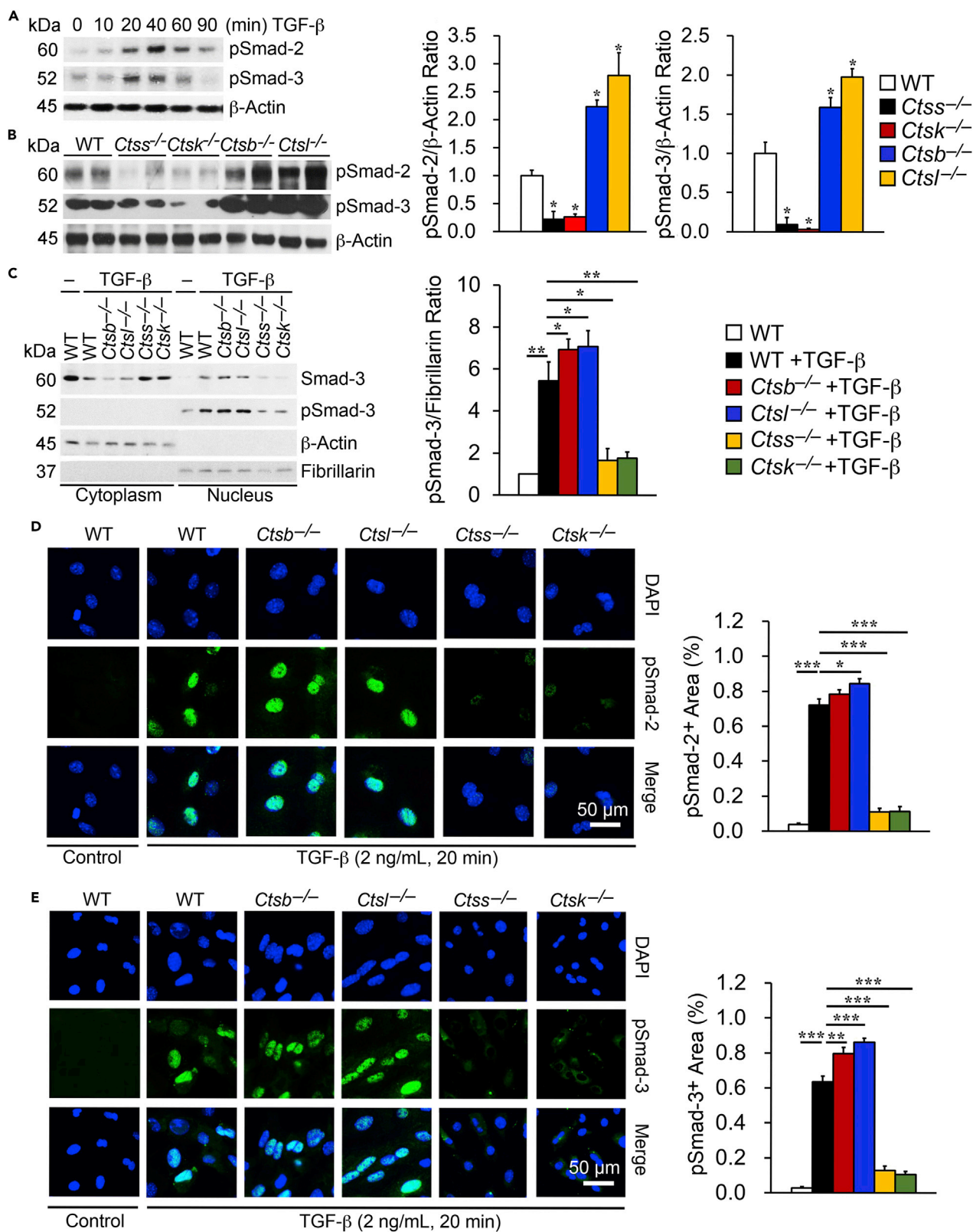


Figure 2. Cathepsin Activity Regulates TGF- β (2 ng/mL) Downstream Smad-2 and Smad-3 Activation in Mouse Kidney TECs

(A) Immunoblot analysis of pSmad-2 and pSmad-3 in kidney TECs with and without TGF- β stimulation at different time points.

(B) Immunoblot analysis of pSmad-2 and pSmad-3 and quantification relative to β -Actin in kidney TECs from WT, *Ctsb*^{-/-}, *Ctsl*^{-/-}, *Ctss*^{-/-}, and *Ctsk*^{-/-} mice after TGF- β stimulation for 20 min.

(C–E) (C) Immunoblot analysis of Smad-3 and pSmad-3 in the cytoplasm and nucleus and quantification of nuclear pSmad-3 relative to fibrillarin after TGF- β stimulation for 20 min in different kidney TECs. Immunofluorescence staining of pSmad-2 (D, green) and pSmad-3 (E, green) with nuclei counterstained with DAPI (blue) and quantification of positive areas. Scale bar: 50 μ m.

Data are representative of four independent experiments. * $p < 0.05$, ** $p < 0.01$, *** $p < 0.001$.

CatB and CatL inhibited pSmad-2/3 nuclear translocation but that CatS and CatK promoted pSmad-2/3 nuclear translocation.

Cathepsin Activities in Nuclear Membrane Transporter Protein Expression and Immunocomplex Formation

Activated Smad-2/3 and common Smad-4 form a complex that possess intrinsic nucleocytoplasmic shuttling capacity to control its target gene transcriptional activities by changing its subcellular distribution (Feng and Derynck, 2005). Nuclear membrane transport factors mediate this process, such as importin- β and RanBP3, which recognize and bind directly to the complex to trigger its nuclear import and export translocations (Dai et al., 2009; Xiao et al., 2000). Results showed increased importin- β expression in TGF- β -activated TECs from *Ctsb*^{-/-} and *Ctsl*^{-/-} mice but decreased expression in TECs from *Ctss*^{-/-} and *Ctsk*^{-/-} mice via immunofluorescent staining and immunoblot analysis (Figures 3A and 3B). Changes in importin- β expression in TECs may affect directly pSmad-2/3 nuclear import (Xiao et al., 2000). In contrast, TECs from *Ctsb*^{-/-} and *Ctsl*^{-/-} mice showed reduced nuclear exporter RanBP3, although CatS- and CatK-deficiency in TECs did not affect RanBP3 expression (Figures 3A and 3B). These observations agree with the increased pSmad-2/3 in the nucleus of TECs from *Ctsb*^{-/-} and *Ctsl*^{-/-} mice and reduced nucleus pSmad-2/3 in TECs from *Ctss*^{-/-} and *Ctsk*^{-/-} mice (Figures 2B–2E). To test whether these cathepsins might interact with importin- β and RanBP3 differently, we performed immunoprecipitation with importin- β or RanBP3 antibodies, followed by immunoblotting with antibodies that recognize different cathepsins. CatS and CatK, but negligibly CatB and CatL, interacted with the nuclear membrane importer importin- β and formed immunocomplexes (Figure 3C). Similarly, CatS or CatK interacted with the nuclear exporter RanBP3 and formed immunocomplexes to a much greater extent than did CatB or CatL (Figure 3D). TGF- β increased the formation of these immunocomplexes (Figures 3C and 3D). These results suggest that CatS or CatK facilitated pSmad-2/3 nuclear-cytoplasmic shuttling more efficiently than did CatB or CatL. Immunofluorescent double staining co-localized these cathepsins to nuclear membrane importin- β and RanBP3 (Figure S2). Therefore, co-localization between cathepsins and importin- β and RanBP3 by immunofluorescent double staining does not necessarily mean their interaction and immunocomplex formation between cathepsins and these nuclear membrane proteins may not indicate their direct or indirect interactions.

Cathepsin Activities in Plasma Membrane TGF- β Receptor Expression and Immunocomplex Formation

Different activities of cathepsins in nuclear membrane importin- β , RanBP3 expression, and immunocomplex formation (Figure 3) may explain the differences of these cathepsins in Smad activation and ECM expression (Figure 2). We further tested whether these cathepsins also interact with TGF- β receptors differently, which may represent another layer of regulation of TGF- β signaling and Smad activation by cathepsins. TGF- β binds and activates TGFBR2, followed by recruiting and activating TGFBR1, essential for downstream Smad-dependent fibrotic signaling and tissue fibrosis (Massague, 1998; Roberts, 1998; Schnaper et al., 2002). In the absence of TGF- β , C-terminal tyrosine residues of TGFBR2 are dephosphorylated by T cell protein tyrosine phosphatase (TCPTP), resulting in TGFBR-dependent inhibition of fibrotic signaling (Chen et al., 2014). Therefore, TCPTP negatively regulates TGFBR2 (Allison, 2014). Immunoprecipitation of TEC lysate from WT mice with anti-TGFBR1 and anti-TGFBR2 antibodies followed by cathepsin immunoblot analysis demonstrated that CatB and CatL formed immunocomplexes with the TGFBR1, whereas CatS and CatK preferentially formed immunocomplexes with the TGFBR2. TGF- β enhanced the formation of these cathepsin-TGFBR immunocomplexes (Figures 4A and 4B). Immunofluorescent double staining co-localized these cathepsins to TGF- β receptors TGFBR1 and TGFBR2 in TECs after TGF- β activation (Figure S3), although the interactions between TGFBR1 and CatS or CatK and between TGFBR2 and CatB and CatL remained negligible by immunoblot analysis (Figures 4A and 4B). Consistent with enhanced interactions between TGFBR1 and CatB or CatL, TGF- β -induced serine phosphorylation on TGFBR1

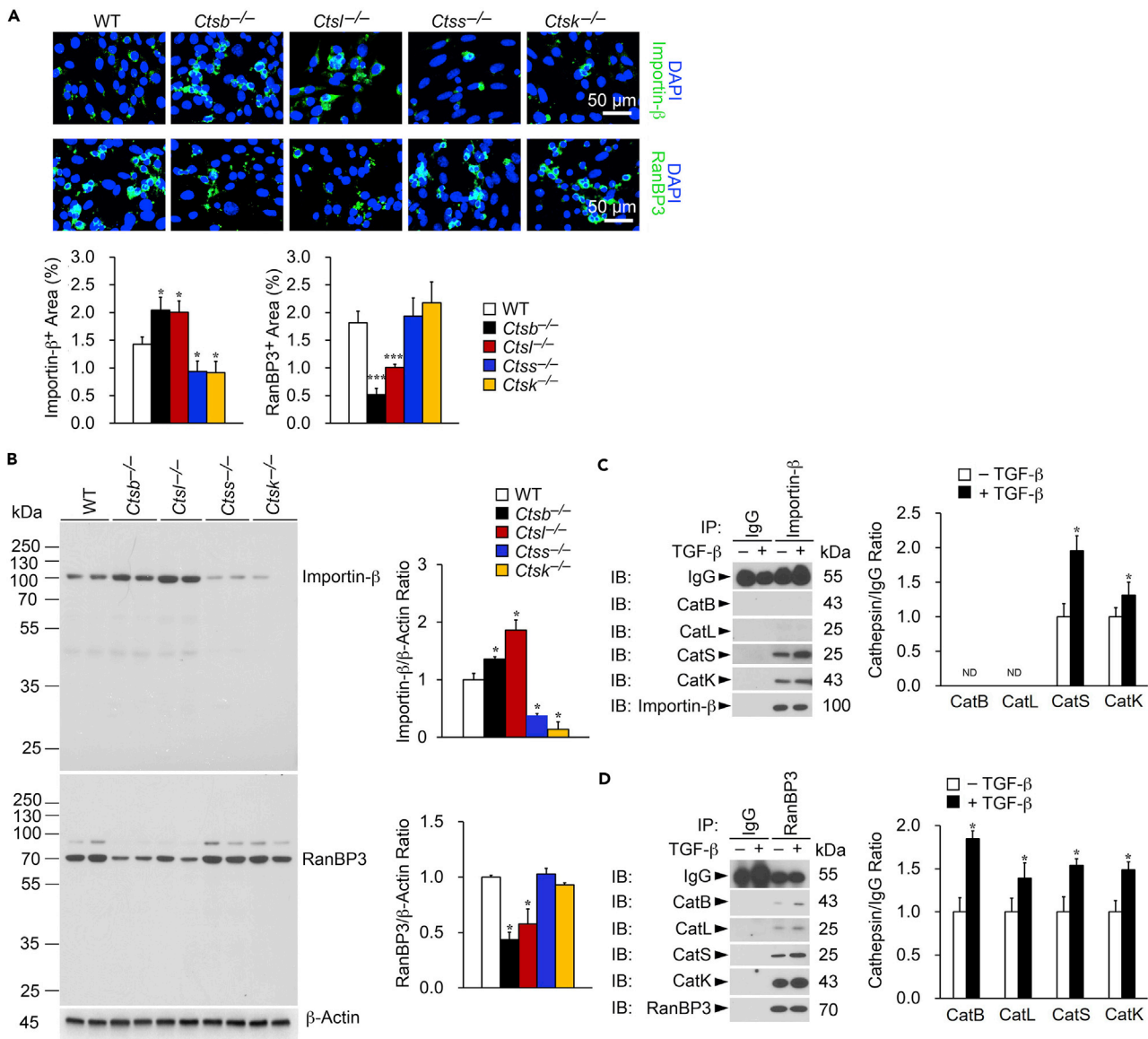


Figure 3. Differential Roles of Cathepsins in Expression and Immunocomplex Formation with Nuclei Membrane Transporters Importin-β and RanBP3

(A–D) Immunofluorescent staining of importin-β (green) and RanBP3 (green) with nuclei counterstained with DAPI (blue) and quantification of positive areas (A) and immunoblot of importin-β and RanBP3 and quantification relative to β-Actin (B) in TECs from different mice as indicated after TGF-β stimulation (2 ng/mL). Immunoprecipitation of anti-importin-β (C) and anti-RanBP-3 (D) of TEC lysates (250 μg), followed by immunoblot detection of different cathepsins and quantification relative to IgG isotype. Mouse IgG isotype (10 μg) was used for immunoprecipitation negative controls. Scale bar: 50 μm. Data are representative of four independent experiments. *p < 0.05, **p < 0.01, ***p < 0.001.

increased in TECs from *Ctsb*^{-/-} and *Ctsl*^{-/-} mice, as determined by TGFBR1 immunoprecipitation followed by anti-p-serine (p-Ser) monoclonal antibody immunoblot analysis. TGFBR1 immunoblot helped ensure equal TGFBR1 immunoprecipitation (Figure 4C). These observations suggest a role of CatB and CatL in interacting with and inhibiting TGFBR1 activation. Absence of any one of them increased TGFBR1 serine phosphorylation. Double deficiency of both CatB and CatL may further increase TGFBR1 activation, although this study did not test this possibility. In contrast, it is also possible that the remaining CatB in TECs from *Ctsl*^{-/-} mice or the remaining CatL in TECs from *Ctsb*^{-/-} mice may bind and activate TGFBR1. Yet, increased TGFBR1 serine phosphorylation in TECs from *Ctsl*^{-/-} or *Ctsb*^{-/-} mice may not support this possibility. TGFBR2 activation in TECs was assessed by TGFBR2 immunoprecipitation of TEC lysates followed by immunoblot analysis of tyrosine phosphorylation (p-Tyr) using an anti-p-Tyr monoclonal

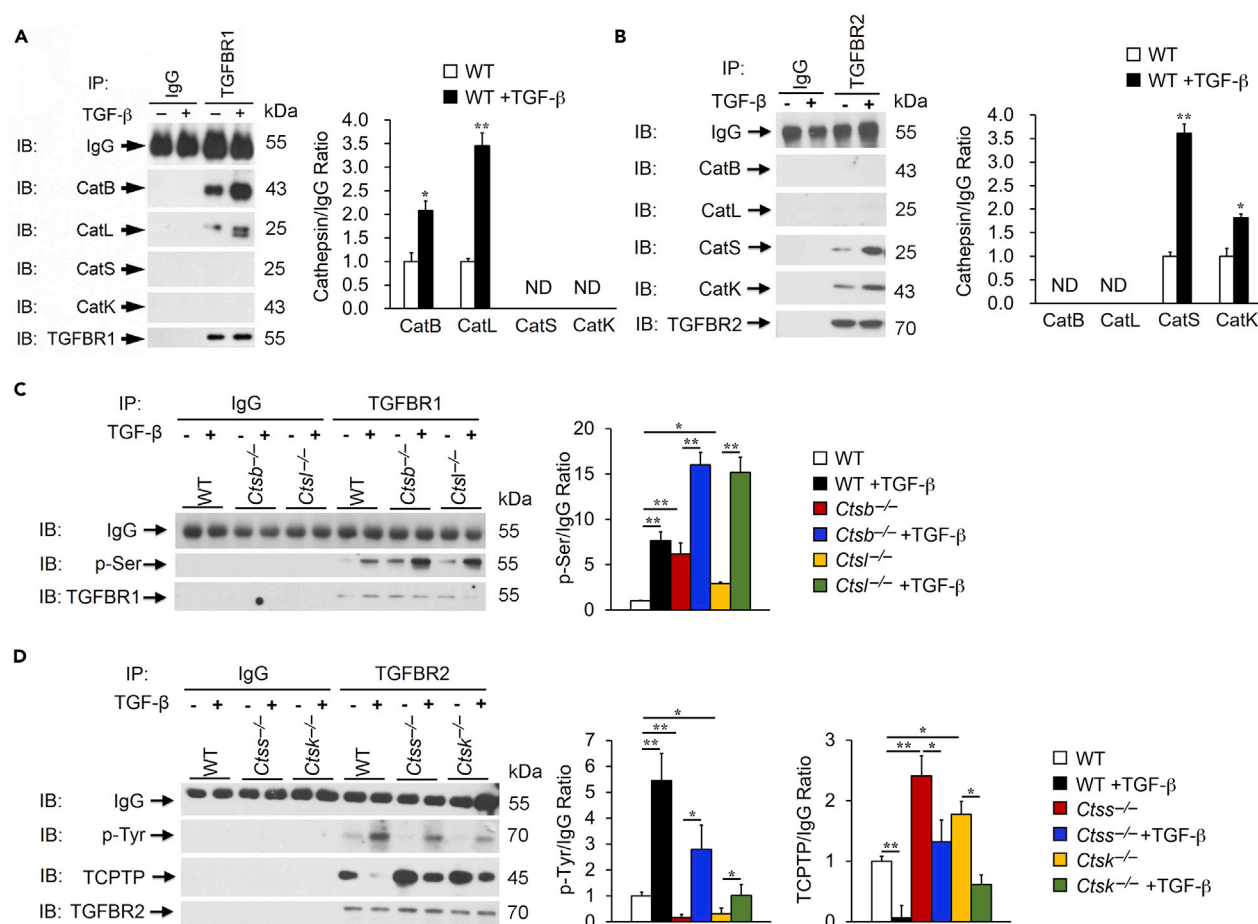


Figure 4. Differential Roles of Cathepsins in Immunocomplex Formation with and Activation of TGF- β Receptor-1 (TGFBFR1) and TGF- β Receptor-2 (TGFBFR2)

(A and B) Immunoprecipitation of TGFBFR1 (A) and TGFBFR2 (B) of WT kidney TECs treated with or without TGF- β were followed by immunoblot analysis of different cathepsins as indicated and quantification relative to IgG. Goat IgG isotype was used as experimental negative control.

(C) TGFBFR1 immunoprecipitation followed by p-Ser and TGFBFR1 immunoblot analysis to detect serine phosphorylation of TGFBFR1 from TECs from WT, *Ctsb*^{-/-}, and *Ctsl*^{-/-} mouse kidneys with and without TGF- β stimulation and quantification relative to IgG isotype.

(D) TGFBFR2 immunoprecipitation followed by p-Tyr, TGFBFR1, and TCPTP immunoblot analyses to detect tyrosine phosphorylation of TGFBFR1 and TGFBFR2-TCPTP complex formation in TECs from WT, *Ctss*^{-/-}, and *Ctsk*^{-/-} kidneys with and without TGF- β stimulation and quantification relative to IgG isotype.

Data representative of four independent experiments. **p* < 0.05, ***p* < 0.01.

antibody. TGF- β -induced p-Tyr on TGFBFR2 decreased in TECs from *Ctss*^{-/-} and *Ctsk*^{-/-} mice, compared with TECs from WT control mice (Figure 4D), suggesting a role of CatS and CatK in interacting and activating TGFBFR2. Consistent with this hypothesis, elevated interaction of TGFBFR2 with its inhibitor TCPTP in TECs from *Ctss*^{-/-} and *Ctsk*^{-/-} mice before and after TGF- β induction was revealed by TGFBFR2 immunoprecipitation followed by immunoblot analysis using the anti-TCPTP antibody. TGFBFR2 immunoblot helped ensure equal TGFBFR2 precipitation (Figure 4D).

TEC Cathepsin Expression in UUO-Injured Mouse Kidneys

Differential roles of CatS and CatK versus CatB and CatL in profibrotic protein production (Figure 1), Smad activation (Figure 2), interactions with nuclear membrane Smad transporter proteins (Figure 3), and interactions with plasma membrane TGF- β receptors (Figure 4) all suggest that these cathepsins contribute differently to tissue fibrosis. To test this conjecture in a fibrosis-dependent pathological process *in vivo* we studied obstructive uropathy in mice. UUO is used broadly to study kidney progressive proximal tubule injury and fibrosis and their underlying mechanisms (Bonventre, 2014; Humphreys et al., 2013; Li et al., 2016; Lovisa et al., 2015; Yang et al., 2010; Zhou et al., 2010). After 14 days, UUO caused extensive proximal tubular degeneration and apoptosis, as determined by loss of E-cadherin immunoreactivity and increase

of TUNEL-positive cells (Figures S4A and S4B), which accompany collecting duct dilatation (Figure S4A) and interstitial fibrosis (Forbes et al., 2011, 2012). Recent studies showed that CatK and CatS contributed to ischemia- or hypoxia-induced vascular cell apoptosis via the Notch1, PPAR- γ , HADC6, and MAPK pathways (Jiang et al., 2014; Li et al., 2015; Wu et al., 2016). Consistent with these hypotheses, we detected many fewer TUNEL-positive cells in the kidneys from *Ctss*^{-/-} and *Ctsk*^{-/-} mice than in those from WT mice after UUU injury (Figure S4B). Immunofluorescent staining also demonstrated the loss of proximal tubular aquaporin-1 expression and an increase of cleaved caspase-3-positive apoptotic cells (Figure S4C). Mouse kidneys after UUU-induced injury showed reduced CatB and CatL activities but increased CatS and CatK activities, as determined by cathepsin active site labeling with biotinylated-JPM (Chen et al., 2013; Sun et al., 2011, 2012) (Figure 5A). Immunostaining revealed the expression of these cathepsins in the proximal tubules in normal mouse kidneys (Figure S5). Immunostaining also localized these cathepsins mainly to the proximal tubules in UUU-injured kidneys (Figures 5B–5E). Some cells in the glomeruli were CatS- and CatK-positive and these cells may be inflammatory infiltrates, yet not defined (Figures 5D and 5E). Immunofluorescent double staining further localized cathepsins to aquaporin-1-positive proximal renal TECs (Jenq et al., 1999; Wang et al., 2015) in UUU-injured kidneys (Figure 5F). Although not tested in this study, inflammatory cell infiltration and expression of CatS and CatK in the glomeruli may also contribute to the kidney fibrosis after UUU injury or other pathological stimuli (Cheng et al., 2011) with different mechanisms from regulating the TEC TGF- β signaling pathway.

Differential Roles of Cathepsins in UUU-Induced Kidney Fibrosis

UUU-induced kidney injury leads to extensive interstitial fibrosis (Forbes et al., 2012). Reduced CatB or CatL activity but increased CatS or CatK activity in UUU-injured kidneys (Figure 5A) suggest their differential roles in post-UUU injury kidney fibrosis. H&E (Figure 6A) and Sirius red staining (Figure 6B) revealed that *Ctsb*^{-/-} and *Ctsl*^{-/-} mice developed greater tubular dilatation and collagen deposition than WT control mice, yet *Ctss*^{-/-} and *Ctsk*^{-/-} mice were protected from post-UUU tubular dilatation and collagen deposition. Immunostaining (Figure 6C) and immunoblot analyses (Figure 6D) supported these conclusions. UUU induced kidney production of the myofibroblast marker α -SMA (LeBleu et al., 2013) and ECM proteins fibronectin, collagen type-I (Col-I), and type-IV (Col-IV) in WT mice. Kidneys from *Ctsb*^{-/-} and *Ctsl*^{-/-} mice showed greatly enhanced accumulation of these ECM constituents, in contrast to those from *Ctss*^{-/-} and *Ctsk*^{-/-} mice. Increased α -SMA expression in kidneys from UUU-treated mice suggests enhanced TEC-to-myofibroblast transition. Kidney zonula occludens-1 (ZO-1)-positive (Figure 7A) and E-cadherin-positive (Figure S6) TEC levels appeared reduced in kidneys from UUU-treated WT mice and further reduced in kidneys from *Ctsb*^{-/-} and *Ctsl*^{-/-} mice. In contrast, ZO-1- and E-cadherin-positive TECs in kidneys from UUU-treated *Ctss*^{-/-} and *Ctsk*^{-/-} mice underwent greater preservation than those in WT mice (Figures 7A and S6), consistent with their reduced kidney α -SMA (Figures 6C and 6D). Kidneys from UUU-treated WT mice also showed increased TGF- β receptors TGFBR1 and TGFBR2, and pSmad-2/3. Such increases were further enhanced in kidneys from UUU-treated *Ctsb*^{-/-} and *Ctsl*^{-/-} mice but blunted in kidneys from *Ctss*^{-/-} and *Ctsk*^{-/-} mice, as determined by both immunoblot analysis and immunostaining (Figures 7B–7D).

DISCUSSION

This study presents differential activities of prominent members of the cathepsin family in interacting with the plasma membrane TGF- β receptors and nuclear membrane transporters. Both properties may contribute to their differential activities in Smad activation, ECM production, and kidney fibrosis from cultured mouse kidney TECs and UUU-induced kidney injury in mice. On the cell membrane, TGF- β interacts with and activates TGFBR2. Activated TGFBR2 mediates TGFBR1 activation. During this process, TCPTP dephosphorylates the p-tyrosine residues located on the C-terminal intracellular tail of the TGFBR2 and acts as a TGFBR2 negative regulator (Chen et al., 2014). Therefore, any molecule that interacts with TGFBR2, TGFBR1, or TCPTP may affect the TGF- β signaling cascade.

This study showed that CatS or CatK formed immunocomplexes with TGFBR2 (Figure 4B). Although immunocomplex formation does not prove direct interaction between cathepsins and TGFBR2, reduced downstream Smad activation (Figures 2B, 2D, and 2E) in TECs from *Ctss*^{-/-} and *Ctsk*^{-/-} mice and reduced kidney ECM production from these mice support the functional consequences of this interaction (Figures 6B–6D). Current evidence does not explain why the interaction between CatS and CatK and TGFBR2 enhanced the downstream TGF- β signaling. Several possibilities may remain. As proteases, CatS and CatK may bind to TGFBR2 and mediate TGFBR2 proteolytic activation. Yet, immunoblot analysis of kidney extracts from *Ctss*^{-/-} and *Ctsk*^{-/-} mice did not detect accumulation of any fragments higher than the predicted 70-kDa

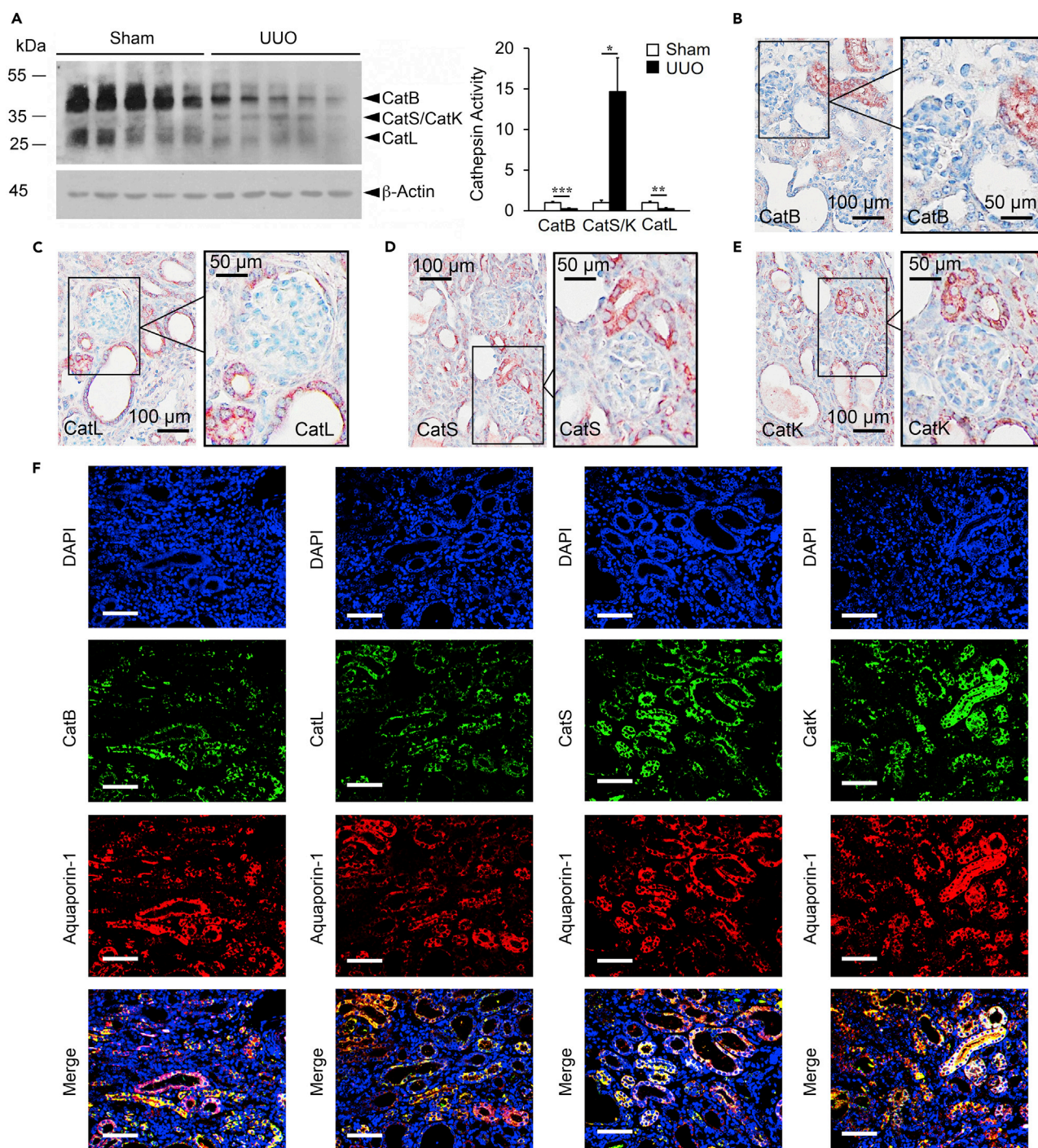


Figure 5. Cathepsin Expression and Localization to TECs in Kidneys from UUO-Injured WT Mice

(A) Kidney tissue extract JPM labeling to detect active cathepsins and quantification relative to β -Actin at 14 days after sham or UUO injury.

(B) Immunostaining of kidney sections to detect the expression of cathepsin B in UUO-treated kidneys. Scale: 100 μ m; Inset scale: 50 μ m.

(C) Immunostaining of kidney sections to detect the expression of cathepsin L in UUO-treated kidneys. Scale: 100 μ m; Inset scale: 50 μ m.

(D) Immunostaining of kidney sections to detect the expression of cathepsin S in UUO-treated kidneys. Scale: 100 μ m; Inset scale: 50 μ m.

(E) Immunostaining of kidney sections to detect the expression of cathepsin K in UUO-treated kidneys. Scale: 100 μ m; Inset scale: 50 μ m.

(F) Immunofluorescent double staining of cathepsins (green) and renal TEC marker aquaporin-1 (red), with nuclei counterstained with DAPI (blue). Scale bar: 100 μ m. n = 8–10 per group. *p < 0.05, **p < 0.01, ***p < 0.001.

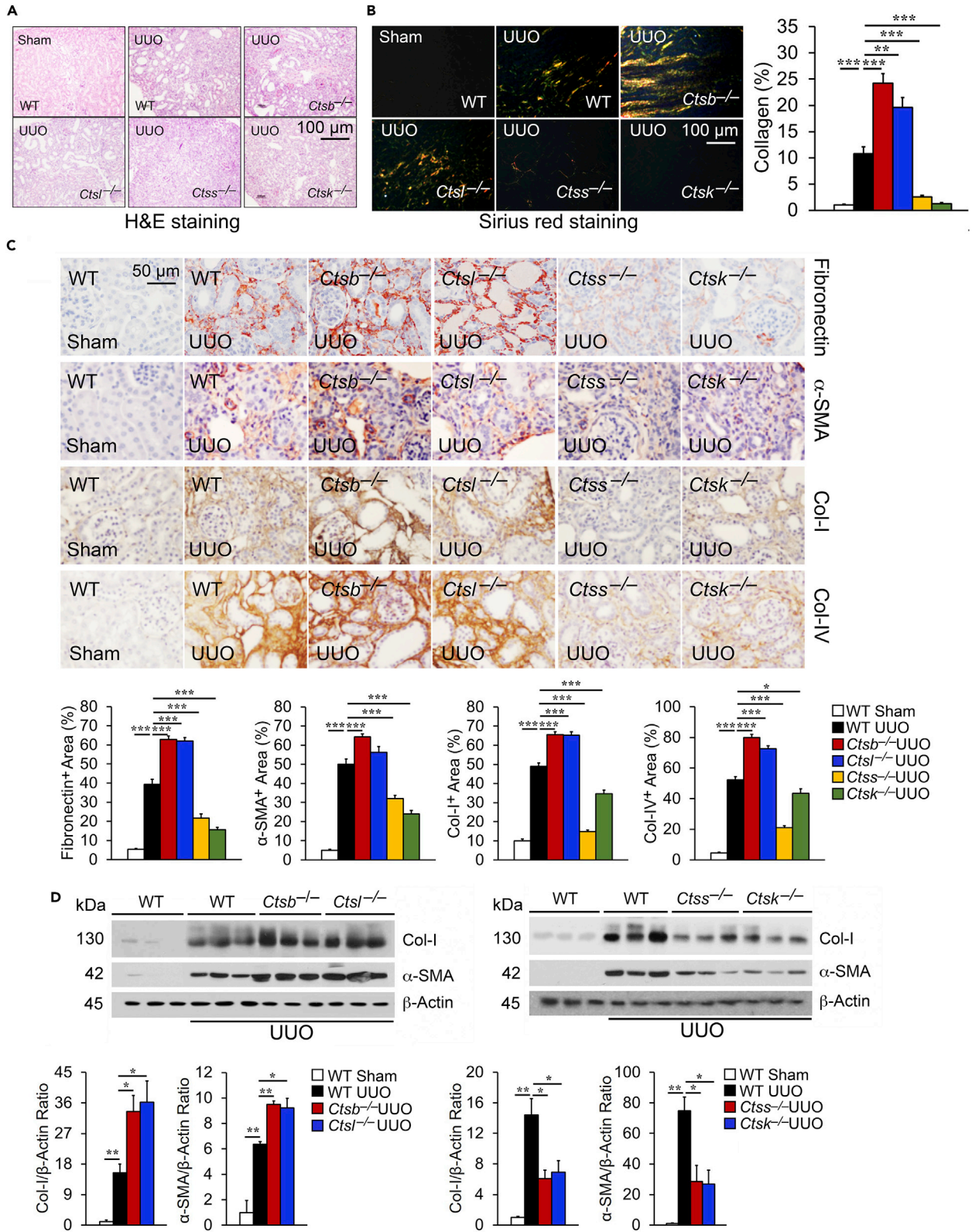


Figure 6. Differential Roles of Cathepsins in Mouse Post-UUO Renal Fibrosis

(A–D) HandE (A) and Sirius red staining and quantification of positive areas (B) of kidneys from sham WT or 14 days post-UUO-treated WT, *Ctsb*^{-/-}, *Ctsl*^{-/-}, *Ctss*^{-/-}, and *Ctsk*^{-/-} mice. Immunostaining (C) and immunoblots (D) detected matrix proteins fibronectin, α -SMA, collagen-I, and collagen-IV and quantification in kidneys from the same sets of mice. Scale bar in (A) and (D): 100 μ m. Scale bar in (C): 50 μ m. n = 8–10 per group. *p < 0.05, **p < 0.01, ***p < 0.001.

TGFBR2 (data not shown), although it is still possible that the monoclonal antibody that recognizes the Ile24 to Asp184 fragment of TGFBR2 may have weak immunoreactivity to the unprocessed TGFBR2 precursors. CatS and CatK may also compete the binding of TGFBR2 with TCPTP. The absence of CatS or CatK gave more chances for TCPTP to attack and suppress TGFBR2 activity. Our data in Figure 4D supported this possibility. In the presence or absence of TGF- β , we detected much more TGFBR2-bound TCPTP in TECs from *Ctss*^{-/-} and *Ctsk*^{-/-} mice than those from WT mice. CatS and CatK expression may also enhance the production of TGFBR2 at the transcriptional or translational levels. Data presented in Figure 7C may support this possibility. Kidneys from *Ctss*^{-/-} and *Ctsk*^{-/-} mice showed reduction of TGFBR2. Yet, the magnitude of reductions of downstream ECM production (Figure 1D) and nuclear pSmad-2/3 translocation (Figures 2B–2E) in TECs from *Ctss*^{-/-} and *Ctsk*^{-/-} mice support the hypothesis that CatS and CatK compete the interaction of TGFBR2 with TCPTP. Therefore, TECs from *Ctss*^{-/-} and *Ctsk*^{-/-} mice showed increased TCPTP binding on TGFBR2 and reduced p-Tyr of TGFBR2 (Figure 4D). In contrast, CatB and CatL acted differently from CatS and CatK. The interaction between CatB and CatL and TGFBR1 (Figure 4A) reduced TGFBR1 activity (p-Ser) (Figure 4C). These data suggest that CatB and CatL negatively regulate TGFBR1. Plasma membrane CatB and CatL may mediate TGFBR1 degradation, which could explain the increased TGFBR1 in kidney extracts from *Ctsb*^{-/-} and *Ctsl*^{-/-} mice (Figure 7B). Alternatively, the formation of immunocomplexes between CatB and CatL and TGFBR1 may prevent the interaction between TGFBR1 and TGFBR2, another site of interference with downstream signaling. The absence of CatB and CatL may facilitate the interaction between the two receptors on the plasma membrane.

On the nuclear membrane, importin- β mediates pSmad-3 translocation from the cytoplasm to the nucleus by binding to pSmad-3 (Xiao et al., 2000). In contrast, RanBP3 exports Smad-2/3 complex also by binding to the Smad-2/3 complex after dephosphorylation by a serine/threonine phosphatase PPM1A as a mechanism to terminate Smad signaling (Dai et al., 2009). Therefore, any interference of importin- β and RanBP3, including expressional changes of these nuclear membrane transporters, may affect their binding with pSmad-2/3 or Smad-2/3, thereby changing the translocation efficiency of Smad complexes. This study showed that CatS and CatK promoted importin- β expression but that CatB and CatL inhibited importin- β expression (Figures 3A and 3B top panel). These expression profile changes may explain enhanced nuclear pSmad-2/3 in TECs from *Ctsb*^{-/-} and *Ctsl*^{-/-} mice and suppressed nuclear pSmad-2/3 in TECs from *Ctss*^{-/-} and *Ctsk*^{-/-} mice (Figures 2B–2E). In contrast to importin- β , RanBP3 showed a reduced expression in TECs from *Ctsb*^{-/-} and *Ctsl*^{-/-} mice but not in those from *Ctss*^{-/-} and *Ctsk*^{-/-} mice (Figure 3B bottom panel), suggesting that only CatB and CatL increased RanBP3 expression, which may increase Smad-2/3 export from the nucleus to cytoplasm, thereby reducing nuclear pSmad-2/3 activity.

This study showed that cathepsin activities regulate the expression of importin- β , RanBP3, TGFBR1, and TGFBR2 (Figure 3A, 3B, 7B, and 7C). How cathepsins controlled the expression of these genes remains unexplained. This situation resembles that we encountered when we found that CatS-deficiency affected the expression of α -SMA (Chen et al., 2013) and CatK- or CatL-deficiency affected the expression of other proteases (Chen et al., 2013; Sun et al., 2011, 2012). We now can explain that CatS-deficiency reduced α -SMA expression by controlling the expression and activities of importin- β , RanBP3, TGFBR1, and TGFBR2. Therefore, cathepsins may also control the transcriptional or translational machineries for other proteases (Sun et al., 2011, 2012).

In addition to enhance importin- β expression, CatS and CatK also preferred to interact or form immunocomplexes with importin- β (Figure 3C) and RanBP3 (Figure 3D) than did CatB and CatL, although CatB and CatL also colocalized to importin- β and RanBP3 by immunofluorescent double staining (Figure S2). Formation of immunocomplexes of CatS and CatK with importin- β may enhance the binding of pSmad-2/3 (Xiao et al., 2000) or increase the translocation efficiency of importin- β . The formation of immunocomplexes of CatS and CatK with RanBP3 may also affect the rate or efficiency of RanBP3 in nuclear protein export. As proteases, CatS and CatK interaction with RanBP3 may affect RanBP3 proteolytic processing or degradation. Yet, no evidence currently exists to support this notion. Immunoblot analysis of RanBP3 in TECs from *Ctss*^{-/-} and *Ctsk*^{-/-} mice did not detect accumulation of the 70-kDa RanBP3 or its precursors

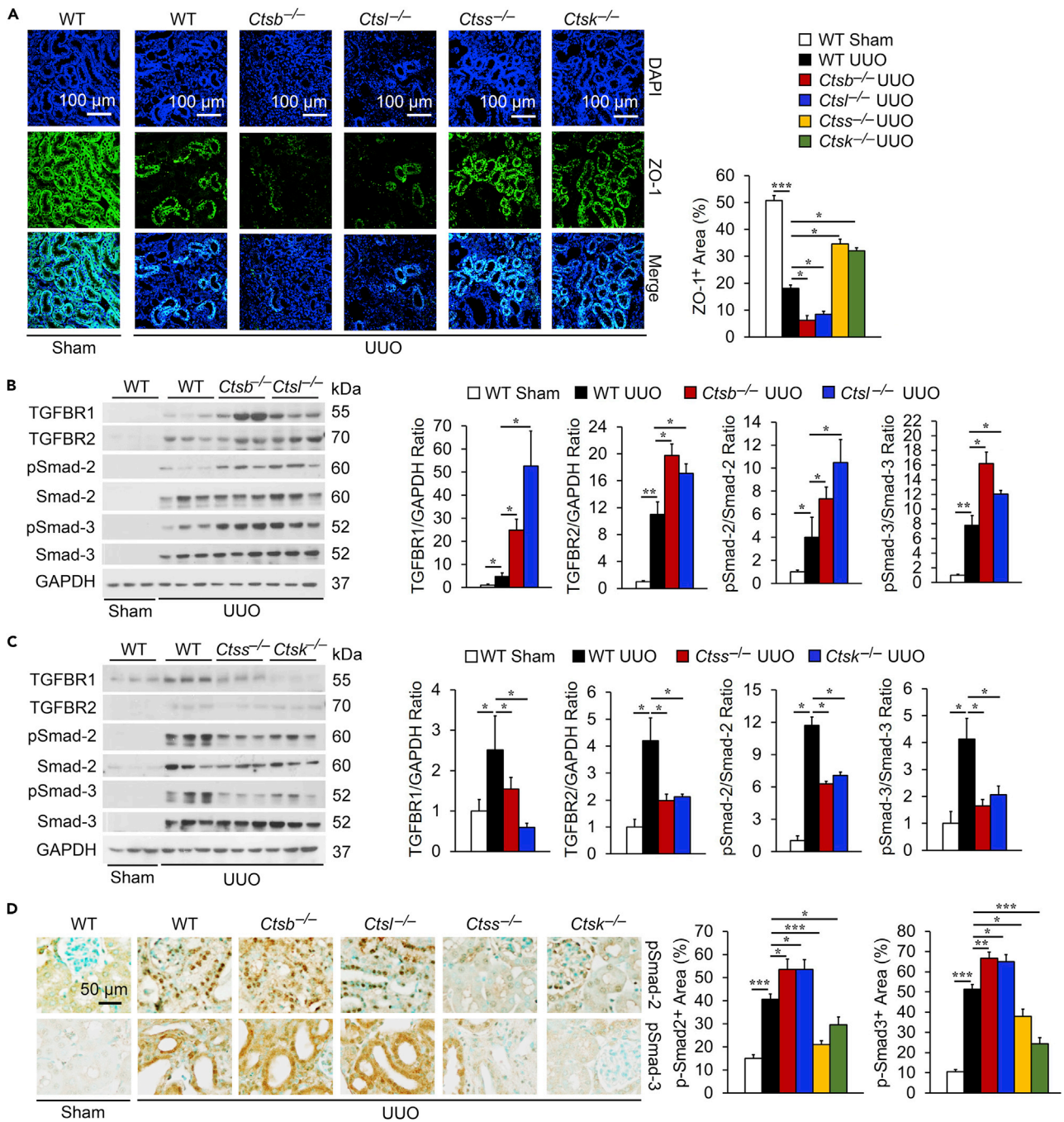


Figure 7. Differential Role of Cathepsins in UUO-Induced Kidney Fibrosis

(A) Immunofluorescent staining of epithelial cell marker ZO-1 (green) with nuclei counterstained with DAPI (blue) in kidneys from sham WT or 14 days post-UUO WT, *Ctsb*^{-/-}, *Ctstl*^{-/-}, *Ctss*^{-/-}, and *Ctsk*^{-/-} mice and quantification of positive areas.

(B) Immunoblot analysis of TGFBR1, TGFBR2, pSmad-2, and pSmad-3 and quantification relative to GAPDH in kidney extracts from sham WT or 14 days post-UUO WT, *Ctsb*^{-/-}, and *Ctstl*^{-/-} mice.

(C) Immunoblot analysis of TGFBR1, TGFBR2, pSmad-2, and pSmad-3 and quantification relative to GAPDH in kidney extracts from sham WT or 14 days post-UUO WT, *Ctss*^{-/-}, and *Ctsk*^{-/-} mice.

(D) Immunostaining of pSmad-2 and pSmad-3 in kidneys from the same sets of mice and quantification of positive areas.

Scale in A: 100 μm. Scale in D: 50 μm. n = 8–10 per group. *p < 0.05, **p < 0.01, ***p < 0.001.

(Figure 3B). Together, our data did not support a major role of CatS and CatK or CatB and CatL in the proteolysis of importin- β or RanBP3, but rather formed immunocomplexes with or affected the expression of these nuclear membrane transporters, thereby facilitating pSmad-2/3 translocation by CatS and CatK or reducing pSmad-2/3 translocation by CatB and CatL. Of note, CatS- and CatK-induced TGF- β signaling may in turn increase the expression of CatS and CatK. CatB- and CatL-reduced TGF- β signaling may also reduce the expression of CatB and CatL (Figures 1A and 1B). Such reciprocal regulation occurred in mouse TECs. Future studies will explore further how and why TGF- β controlled differently the expression of CatS and CatK versus CatB and CatL.

The influences of cathepsins on tissue fibrosis may vary depending on the type of cathepsins, disease states, and cell types. In contrast to the present results regarding kidney fibrosis and TECs, CatK expression reduces lung and cardiac fibrosis. CatK deficiency exacerbated lung fibrosis, myocardial fibrosis, and cardiomyopathy (Buhling et al., 2004; Petermann et al., 2006; Zhang et al., 2011b). CatK overexpression limited these findings (Srivastava et al., 2008; Tang et al., 2009; Zhang et al., 2011a). TGF- β reduced CatK expression in fibroblasts (van den Brule et al., 2005) and CatL expression in lung epithelial cells (Chen et al., 2013). In contrast, CatB expression seems to promote lung and liver fibrosis. In human lung fibroblasts, CatB inhibition delayed fibroblast differentiation, decreased pSmad-2/3, and diminished α -SMA expression (Kasabova et al., 2014). CatB inhibition reduced CCl₄-induced liver fibrosis (Moles et al., 2009, 2012). In our recent study of diet-induced nonalcoholic fatty liver disease (Wang et al., 2016), we found that CatB-deficiency reduced liver fibrosis (G.-P.S., Unpublished Data). Therefore, cathepsin activities in TGF- β signaling and tissue fibrosis may have disease-type- and cell-type-dependent properties.

Together, this study established differential roles of cathepsins in TGF- β signaling and renal fibrosis. The study also suggests that, instead of targeting cathepsins, mitigating tissue fibrosis by targeting TGF- β or its receptors may prove safer (Hill et al., 2001; Moon et al., 2006; Petersen et al., 2008; Russo et al., 2007), such as anti-TGF- β neutralizing antibody, endoglin (a TGF- β binding protein) antibody, soluble TGF- β type-II receptor, TGF- β antisense oligonucleotide, specific inhibitors of TGF- β receptor kinases (GW788388 and IN-1130), and pirfenidone (a small molecule TGF- β inhibitor), which recently received approval for the treatment of IPF (Carter, 2011). The use of cathepsin inhibitors to treat tissue fibrosis-associated diseases requires considerable caution, as a cathepsin that mitigates fibrosis of a given organ may aggravate fibrosis in other organs. Thus, these results shed mechanistic insight into how these closely related proteinases can exert opposing effects and how they can do so independent of their proteolytic properties. These findings have implications for understanding the regulation of tissue fibrosis in general as well as increasing our knowledge of cysteinyl proteinase biology.

Limitations of the Study

This study reports that cysteinyl proteases cathepsins regulate TGF- β signaling and tissue fibrosis independent of their proteolytic activities. With different activities in regulating the expression of and in binding to the nuclear membrane Smad complex transporters importin- β and RanBP3 and plasma membrane TGF- β receptors TGFBR1 and TGFBR2, CatB and CatL exert opposite activities to those of CatS and CatK in controlling TGF- β signaling and tissue fibrosis. Several study limitations remain. First, we currently do not know how these cathepsins interact with importin- β , RanBP3, TGFBR1, and TGFBR2. This study only shows the immunocomplex formation between cathepsins and those nuclear and plasma membrane proteins. Such interaction may involve direct contact.

Yet, the identity of the specific primary residues responsible for the interaction on cathepsins and membrane proteins remains untested. Alternatively, such interaction can be indirect and involve other untested molecules. This study does not analyze the components from different cathepsin-membrane protein immunocomplexes. Second, this study uses kidney TECs and UUO-induced kidney injury model to study cathepsin activities in tissue fibrosis. It is possible that the observed activities of these cathepsins in kidney TECs may differ from those in other cell types or organs. This study does not test this hypothesis. Third, earlier studies show that deficiency of one cathepsin affects the expression of other cathepsins or matrix metalloproteinases in vascular smooth muscle cells, endothelial cells, and adipocytes (Sun et al., 2011, 2012; Yang et al., 2008). Yet, the underline mechanisms by which cathepsins regulate the expression of other proteases remain unknown because cathepsins have never been implicated in gene expression regulation besides their proteolytic function. This study offers an example that CatB, CatL, CatS, and CatK contribute to tissue fibrosis by regulating TGF- β signaling and ECM protein expression. This activity of

cathepsins involves not only cathepsin immunocomplex formation with importin- β , RanBP3, TGFBR1, and TGFBR2, but also expression regulation of these nuclear and plasma membrane proteins. Yet, how these cathepsins regulate the expression of these membrane proteins remains unresolved.

METHODS

All methods can be found in the accompanying [Transparent Methods supplemental file](#).

SUPPLEMENTAL INFORMATION

Supplemental Information can be found online at <https://doi.org/10.1016/j.isci.2019.08.014>.

ACKNOWLEDGMENTS

The authors thank Ms. Eugenia Shvartz for her technical assistance and Ms. Chelsea Swallow for her editorial assistance. This work is supported by grants from the National Institutes of Health (HL080472 to P.L.; HL123568, HL60942, and AG058670 to G.-P.S.), and the RRM Charitable Fund to P.L. X.Z. is supported by the American Heart Association Postdoctoral Fellowship # 18POST34050043.

AUTHOR CONTRIBUTIONS

X.Z., Y.Z., Q.H., W.F., and J.L. performed all *in vitro* and *in vivo* experiments. G.K.S. helped with the immunostaining experiments. X.Y. supported financially to the project. P.L. helped with the data interpretation and manuscript writing. J.V.B. supported the mouse kidney epithelial cell culture. G.-P.S. designed the experiments and wrote the manuscript.

DECLARATION OF INTERESTS

The authors declare that no conflicts of interest are present.

Received: March 15, 2019

Revised: June 11, 2019

Accepted: August 6, 2019

Published: September 27, 2019

REFERENCES

- Allison, S.J. (2013). Cardiovascular disease: progression of coronary artery calcification in patients with type 1 diabetes mellitus with and without kidney disease. *Nat. Rev. Nephrol.* **9**, 494.
- Allison, S.J. (2014). Fibrosis: regulation of fibrotic signalling by TGF- β receptor tyrosine phosphorylation. *Nat. Rev. Nephrol.* **10**, 484.
- Bonventre, J.V. (2014). Primary proximal tubule injury leads to epithelial cell cycle arrest, fibrosis, vascular rarefaction, and glomerulosclerosis. *Kidney Int. Suppl.* (2011) **4**, 39–44.
- Border, W.A., and Noble, N.A. (1994). Transforming growth factor beta in tissue fibrosis. *N. Engl. J. Med.* **331**, 1286–1292.
- Buhling, F., Rocken, C., Brasch, F., Hartig, R., Yasuda, Y., Saftig, P., Bromme, D., and Welte, T. (2004). Pivotal role of cathepsin K in lung fibrosis. *Am. J. Pathol.* **164**, 2203–2216.
- Bujak, M., Ren, G., Kweon, H.J., Dobaczewski, M., Reddy, A., Taffet, G., Wang, X.F., and Frangogiannis, N.G. (2007). Essential role of Smad3 in infarct healing and in the pathogenesis of cardiac remodeling. *Circulation* **116**, 2127–2138.
- Carter, N.J. (2011). Pirfenidone: in idiopathic pulmonary fibrosis. *Drugs* **71**, 1721–1732.
- Chen, H., Wang, J., Xiang, M.X., Lin, Y., He, A., Jin, C.N., Guan, J., Sukhova, G.K., Libby, P., Wang, J.A., et al. (2013). Cathepsin S-mediated fibroblast trans-differentiation contributes to left ventricular remodelling after myocardial infarction. *Cardiovasc. Res.* **100**, 84–94.
- Chen, X., Wang, H., Liao, H.J., Hu, W., Gewin, L., Mernaugh, G., Zhang, S., Zhang, Z.Y., Vega-Montoto, L., Vanacore, R.M., et al. (2014). Integrin-mediated type II TGF- β receptor tyrosine dephosphorylation controls SMAD-dependent profibrotic signaling. *J. Clin. Invest.* **124**, 3295–3310.
- Cheng, X.W., Kuzuya, M., Sasaki, T., Inoue, A., Hu, L., Song, H., Huang, Z., Li, P., Takeshita, K., Hirashiki, A., et al. (2011). Inhibition of mineralocorticoid receptor is a renoprotective effect of the 3-hydroxy-3-methylglutaryl-coenzyme A reductase inhibitor pitavastatin. *J. Hypertens.* **29**, 542–552.
- Dai, F., Lin, X., Chang, C., and Feng, X.H. (2009). Nuclear export of Smad2 and Smad3 by RanBP3 facilitates termination of TGF- β signaling. *Dev. Cell* **16**, 345–357.
- Dongiovanni, P., Romeo, S., and Valenti, L. (2014). Hepatocellular carcinoma in nonalcoholic fatty liver: role of environmental and genetic factors. *World J. Gastroenterol.* **20**, 12945–12955.
- Eddy, A.A., and Neilson, E.G. (2006). Chronic kidney disease progression. *J. Am. Soc. Nephrol.* **17**, 2964–2966.
- Feng, X.H., and Derynck, R. (2005). Specificity and versatility in TGF- β signaling through Smads. *Annu. Rev. Cell Dev. Biol.* **21**, 659–693.
- Forbes, M.S., Thornhill, B.A., and Chevalier, R.L. (2011). Proximal tubular injury and rapid formation of atubular glomeruli in mice with unilateral ureteral obstruction: a new look at an old model. *Am. J. Physiol. Renal Physiol.* **301**, F110–F117.
- Forbes, M.S., Thornhill, B.A., Minor, J.J., Gordon, K.A., Galarreta, C.I., and Chevalier, R.L. (2012). Fight-or-flight: murine unilateral ureteral obstruction causes extensive proximal tubular degeneration, collecting duct dilatation, and minimal fibrosis. *Am. J. Physiol. Renal Physiol.* **303**, F120–F129.
- Gerber, A., Wille, A., Welte, T., Ansoorge, S., and Buhling, F. (2001). Interleukin-6 and transforming growth factor- β 1 control expression of cathepsins B and L in human lung epithelial cells. *J. Interferon Cytokine Res.* **21**, 11–19.
- Grande, M.T., Sanchez-Laorden, B., Lopez-Blau, C., De Frutos, C.A., Boutet, A., Arealo, M., Rowe, R.G., Weiss, S.J., Lopez-Novoa, J.M., and Nieto, M.A. (2015). Snail1-induced partial epithelial-to-

- mesenchymal transition drives renal fibrosis in mice and can be targeted to reverse established disease. *Nat. Med.* 21, 989–997.
- Harris, W.T., Kelly, D.R., Zhou, Y., Wang, D., MacEwen, M., Hagood, J.S., Clancy, J.P., Ambalavanan, N., and Sorscher, E.J. (2013). Myofibroblast differentiation and enhanced TGF- β signaling in cystic fibrosis lung disease. *PLoS One* 8, e70196.
- Hill, C., Flyvbjerg, A., Rasch, R., Bak, M., and Logan, A. (2001). Transforming growth factor- β 2 antibody attenuates fibrosis in the experimental diabetic rat kidney. *J. Endocrinol.* 170, 647–651.
- Humphreys, B.D., Xu, F., Sabbiseti, V., Grgic, I., Movahedi Naini, S., Wang, N., Chen, G., Xiao, S., Patel, D., Henderson, J.M., et al. (2013). Chronic epithelial kidney injury molecule-1 expression causes murine kidney fibrosis. *J. Clin. Invest.* 123, 4023–4035.
- Jenq, W., Cooper, D.R., Bittle, P., and Ramirez, G. (1999). Aquaporin-1 expression in proximal tubule epithelial cells of human kidney is regulated by hyperosmolarity and contrast agents. *Biochem. Biophys. Res. Commun.* 256, 240–248.
- Jiang, H., Cheng, X.W., Shi, G.P., Hu, L., Inoue, A., Yamamura, Y., Wu, H., Takeshita, K., Li, X., Huang, Z., et al. (2014). Cathepsin K-mediated Notch1 activation contributes to neovascularization in response to hypoxia. *Nat. Commun.* 5, 3838.
- Kasabova, M., Joulin-Giet, A., Lecaille, F., Gilmore, B.F., Marchand-Adam, S., Saidi, A., and Lalmanach, G. (2014). Regulation of TGF- β 1-driven differentiation of human lung fibroblasts: emerging roles of cathepsin B and cystatin C. *J. Biol. Chem.* 289, 16239–16251.
- Kasabova, M., Villeret, B., Gombault, A., Lecaille, F., Reinheckel, T., Marchand-Adam, S., Couillin, I., and Lalmanach, G. (2016). Discordance in cathepsin B and cystatin C expressions in bronchoalveolar fluids between murine bleomycin-induced fibrosis and human idiopathic fibrosis. *Respir. Res.* 17, 118.
- Lan, H.Y. (2003). Tubular epithelial-myofibroblast transdifferentiation mechanisms in proximal tubule cells. *Curr. Opin. Nephrol. Hypertens.* 12, 25–29.
- LeBleu, V.S., Taduri, G., O’Connell, J., Teng, Y., Cooke, V.G., Woda, C., Sugimoto, H., and Kalluri, R. (2013). Origin and function of myofibroblasts in kidney fibrosis. *Nat. Med.* 19, 1047–1053.
- Li, H., Peng, X., Wang, Y., Cao, S., Xiong, L., Fan, J., Wang, Y., Zhuang, S., Yu, X., and Mao, H. (2016). Atg5-mediated autophagy deficiency in proximal tubules promotes cell cycle G2/M arrest and renal fibrosis. *Autophagy* 12, 1472–1486.
- Li, M., Krishnaveni, M.S., Li, C., Zhou, B., Xing, Y., Banfalvi, A., Li, A., Lombardi, V., Akbari, O., Borok, Z., et al. (2011). Epithelium-specific deletion of TGF- β receptor type II protects mice from bleomycin-induced pulmonary fibrosis. *J. Clin. Invest.* 121, 277–287.
- Li, X., Cheng, X.W., Hu, L., Wu, H., Guo, P., Hao, C.N., Jiang, H., Zhu, E., Huang, Z., Inoue, A., et al. (2015). Cathepsin S activity controls ischemia-induced neovascularization in mice. *Int. J. Cardiol.* 183, 198–208.
- Lovisa, S., LeBleu, V.S., Tampe, B., Sugimoto, H., Vadnagara, K., Carstens, J.L., Wu, C.C., Hagos, Y., Burckhardt, B.C., Pentcheva-Hoang, T., et al. (2015). Epithelial-to-mesenchymal transition induces cell cycle arrest and parenchymal damage in renal fibrosis. *Nat. Med.* 21, 998–1009.
- Manchanda, M., Das, P., Gahlot, G.P.S., Singh, R., Roeb, E., Roderfeld, M., Datta Gupta, S., Saraya, A., Pandey, R.M., and Chauhan, S.S. (2017). Cathepsin L and B as potential markers for liver fibrosis: insights from patients and experimental models. *Clin. Transl. Gastroenterol.* 8, e99.
- Massague, J. (1998). TGF- β signal transduction. *Annu. Rev. Biochem.* 67, 753–791.
- Meng, X.M., Nikolic-Paterson, D.J., and Lan, H.Y. (2014). Inflammatory processes in renal fibrosis. *Nat. Rev. Nephrol.* 10, 493–503.
- Moles, A., Tarrats, N., Fernandez-Checa, J.C., and Mari, M. (2009). Cathepsins B and D drive hepatic stellate cell proliferation and promote their fibrogenic potential. *Hepatology* 49, 1297–1307.
- Moles, A., Tarrats, N., Fernandez-Checa, J.C., and Mari, M. (2012). Cathepsin B overexpression due to acid sphingomyelinase ablation promotes liver fibrosis in Niemann-Pick disease. *J. Biol. Chem.* 287, 1178–1188.
- Moon, J.A., Kim, H.T., Cho, I.S., Sheen, Y.Y., and Kim, D.K. (2006). IN-1130, a novel transforming growth factor- β type I receptor kinase (ALK5) inhibitor, suppresses renal fibrosis in obstructive nephropathy. *Kidney Int.* 70, 1234–1243.
- Murray, L.A., Chen, Q., Kramer, M.S., Hesson, D.P., Argentieri, R.L., Peng, X., Gulati, M., Homer, R.J., Russell, T., van Rooijen, N., et al. (2011). TGF- β driven lung fibrosis is macrophage dependent and blocked by Serum amyloid P. *Int. J. Biochem. Cell Biol.* 43, 154–162.
- Nikolic-Paterson, D.J., Wang, S., and Lan, H.Y. (2014). Macrophages promote renal fibrosis through direct and indirect mechanisms. *Kidney Int. Suppl.* (2011) 4, 34–38.
- Petermann, I., Mayer, C., Stypmann, J., Biniossek, M.L., Tobin, D.J., Engelen, M.A., Dandekar, T., Grune, T., Schild, L., Peters, C., et al. (2006). Lysosomal, cytoskeletal, and metabolic alterations in cardiomyopathy of cathepsin L knockout mice. *FASEB J.* 20, 1266–1268.
- Petersen, M., Thorikay, M., Deckers, M., van Dinther, M., Grygielko, E.T., Gellibert, F., de Gouville, A.C., Huet, S., ten Dijke, P., and Laping, N.J. (2008). Oral administration of GW788388, an inhibitor of TGF- β type I and II receptor kinases, decreases renal fibrosis. *Kidney Int.* 73, 705–715.
- Roberts, A.B. (1998). Molecular and cell biology of TGF- β . *Miner. Electrolyte Metab.* 24, 111–119.
- Russo, L.M., del Re, E., Brown, D., and Lin, H.Y. (2007). Evidence for a role of transforming growth factor (TGF)- β 1 in the induction of postglomerular albuminuria in diabetic nephropathy: amelioration by soluble TGF- β type II receptor. *Diabetes* 56, 380–388.
- Schnaper, H.W., Hayashida, T., and Poncelet, A.C. (2002). It’s a Smad world: regulation of TGF- β signaling in the kidney. *J. Am. Soc. Nephrol.* 13, 1126–1128.
- Srivastava, M., Steinwede, K., Kiviranta, R., Morko, J., Hoymann, H.G., Langer, F., Buhling, F., Welte, T., and Maus, U.A. (2008). Overexpression of cathepsin K in mice decreases collagen deposition and lung resistance in response to bleomycin-induced pulmonary fibrosis. *Respir. Res.* 9, 54.
- Sun, J., Sukhova, G.K., Zhang, J., Chen, H., Sjoberg, S., Libby, P., Xia, M., Xiong, N., Gelb, B.D., and Shi, G.P. (2012). Cathepsin K deficiency reduces elastase perfusion-induced abdominal aortic aneurysms in mice. *Arterioscler. Thromb. Vasc. Biol.* 32, 15–23.
- Sun, J., Sukhova, G.K., Zhang, J., Chen, H., Sjoberg, S., Libby, P., Xiang, M., Wang, J., Peters, C., Reinheckel, T., et al. (2011). Cathepsin L activity is essential to elastase perfusion-induced abdominal aortic aneurysms in mice. *Arterioscler. Thromb. Vasc. Biol.* 31, 2500–2508.
- Talasz, A.H., Khalili, H., Jenab, Y., Salarifar, M., Broumand, M.A., and Darabi, F. (2013). N-Acetylcysteine effects on transforming growth factor- β and tumor necrosis factor- α serum levels as pro-fibrotic and inflammatory biomarkers in patients following ST-segment elevation myocardial infarction. *Drugs R D* 13, 199–205.
- Tang, Q., Cai, J., Shen, D., Bian, Z., Yan, L., Wang, Y.X., Lan, J., Zhuang, G.Q., Ma, W.Z., and Wang, W. (2009). Lysosomal cysteine peptidase cathepsin L protects against cardiac hypertrophy through blocking AKT/GSK3 β signaling. *J. Mol. Med. (Berl.)* 87, 249–260.
- van den Brule, S., Misson, P., Buhling, F., Lison, D., and Huaux, F. (2005). Overexpression of cathepsin K during silica-induced lung fibrosis and control by TGF- β . *Respir. Res.* 6, 84.
- Verrecchia, F., Chu, M.L., and Mauviel, A. (2001). Identification of novel TGF- β /Smad gene targets in dermal fibroblasts using a combined cDNA microarray/promoter transactivation approach. *J. Biol. Chem.* 276, 17058–17062.
- Wang, W., Li, F., Sun, Y., Lei, L., Zhou, H., Lei, T., Xia, Y., Verkman, A.S., and Yang, B. (2015). Aquaporin-1 retards renal cyst development in polycystic kidney disease by inhibition of Wnt signaling. *FASEB J.* 29, 1551–1563.
- Wang, X., Zheng, Z., Caviglia, J.M., Corey, K.E., Herfel, T.M., Cai, B., Masia, R., Chung, R.T., Lefkowitz, J.H., Schwabe, R.F., et al. (2016). Hepatocyte TAZ/WWTR1 promotes inflammation and fibrosis in nonalcoholic steatohepatitis. *Cell Metab.* 24, 848–862.
- Wu, H., Cheng, X.W., Hu, L., Takeshita, K., Hu, C., Du, Q., Li, X., Zhu, E., Huang, Z., Yisireyili, M., et al. (2016). Cathepsin S activity controls injury-related vascular repair in mice via the TLR2-mediated p38MAPK and PI3K-Akt/p-HDAC6 signaling pathway. *Arterioscler. Thromb. Vasc. Biol.* 36, 1549–1557.
- Xiao, Z., Liu, X., and Lodish, H.F. (2000). Importin beta mediates nuclear translocation of Smad 3. *J. Biol. Chem.* 275, 23425–23428.
- Yang, L., Besschetnova, T.Y., Brooks, C.R., Shah, J.V., and Bonventre, J.V. (2010). Epithelial cell

cycle arrest in G2/M mediates kidney fibrosis after injury. *Nat. Med.* 16, 535–543, 531p following 143.

Yang, M., Sun, J., Zhang, T., Liu, J., Zhang, J., Shi, M.A., Darakhshan, F., Guerre-Millo, M., Clement, K., Gelb, B.D., et al. (2008). Deficiency and inhibition of cathepsin K reduce body weight gain and increase glucose metabolism in mice. *Arterioscler. Thromb. Vasc. Biol.* 28, 2202–2208.

Zhang, D., Huang, C., Yang, C., Liu, R.J., Wang, J., Niu, J., and Bromme, D. (2011a). Antifibrotic effects of curcumin are associated with overexpression of cathepsins K and L in bleomycin treated mice and human fibroblasts. *Respir. Res.* 12, 154.

Zhang, D., Leung, N., Weber, E., Saftig, P., and Bromme, D. (2011b). The effect of cathepsin K

deficiency on airway development and TGF-beta1 degradation. *Respir. Res.* 12, 72.

Zhou, Y., Mao, H., Li, S., Cao, S., Li, Z., Zhuang, S., Fan, J., Dong, X., Borkan, S.C., Wang, Y., et al. (2010). HSP72 inhibits Smad3 activation and nuclear translocation in renal epithelial-to-mesenchymal transition. *J. Am. Soc. Nephrol.* 21, 598–609.

ISCI, Volume 19

Supplemental Information

Differential Roles of CysteinyI Cathepsins

in TGF- β Signaling and Tissue Fibrosis

Xian Zhang, Yi Zhou, Xueqing Yu, Qin Huang, Wenqian Fang, Jie Li, Joseph V. Bonventre, Galina K. Sukhova, Peter Libby, and Guo-Ping Shi

Supplemental Materials

Differential roles of cysteinyl cathepsins in TGF- β signaling and renal fibrosis

Xian Zhang, Yi Zhou, Xueqing Yu, Qin Huang, Wenqian Fang, Jie Li, Joseph V. Bonventre, Galina K. Sukhova, Peter Libby, Guo-Ping Shi

TRANSPARENT METHODS

Mice

Eight-week-old male *Ctsb*^{-/-} (C57BL/6, N>7), *Ctsl*^{-/-} mice (C57BL/6, N>7), *Cats*^{-/-} (C57BL/6, N>10), *Ctsk*^{-/-} (C57BL/6, N>9) and male wild type (C57BL/6, Jackson Laboratory, Bar Harbor, ME) were kept under pathogen-free conditions and housed in a temperature controlled room with a 12-hour light/dark cycle with ad libitum access to food and water. All animal procedures conformed to the Guide for the Care and Use of Laboratory Animals published by the US National Institutes of Health and were approved by the Harvard Medical School Standing Committee on Animals (protocol #03759). To produce unilateral ureteral obstruction (UUO)-induced kidney fibrosis, we grouped mice randomly into sham or UUO groups. Surgery was performed by exposing the left ureter through a flank incision and then immediately closing the incision (sham) or double-ligating the left ureter with silk sutures (UUO). A minimum of 8~10 mice were used in each experimental group. All mice were sacrificed at 14 days after UUO.

Kidney histology analysis

Mouse kidney tissues were fixed with 4% paraformaldehyde (#P6148, Sigma-Aldrich, St. Louis, MO). Paraffin-embedded 4- μ m kidney sections were prepared and stained with Masson's trichrome (#87019, Thermo Fisher Scientific, Waltham, MA), picosirius red (#24901, Polysciences, Warrington, PA), apoptotic cell detection kit (#S7100, Millipore, Burlington, MA), and hematoxylin and eosin (H&E) (Sigma-Aldrich) according to the instructions. Five random fields/section were examined, and collagen content quantified using Image-Pro Plus.

For immunohistochemical analysis, the kidney sections were deparaffinized, rehydrated and incubated with the following primary antibodies: rabbit anti-cathepsin B (1:50, #PC41, Calbiochem, Billerica, MA), rabbit anti-cathepsin L (1:20, #168-10557, Raybiotech, Norcross, GA), rabbit anti-cathepsin S (was produced by our own group; 1:200), rabbit anti-cathepsin K (1:50, #PB9856, Boster, Pleasanton, CA), mouse anti-fibronectin (1:100, #ab6328, Abcam, Cambridge, MA), rabbit anti- α -SMA (1:750, #A2547, Sigma-Aldrich), rabbit anti-collagen-I (1:100, #ab292, Abcam) and rabbit anti-collagen-IV (1:100, #ab19808, Abcam), rabbit anti-pSmad-2 (1:30, #3108S, Cell Signaling Technology, Danvers, MA), rabbit anti-pSmad-3 (1:30, #9520S, Cell Signaling Technology) and anti-aquaporin-1 (1:100, #sc-9878, Santa Cruz Biotechnology, Dallas, TX), followed by appropriate biotin-conjugated secondary antibodies (1:500, Vector Laboratories, Burlingame, CA) and HRP-streptavidin (#P039701-2, DAKO, Carpinteria, CA). After detection with AEC chromogenic agent (#K3464, DAKO), slides were counterstained with hematoxylin (Sigma-Aldrich). Representative images were acquired with a Leica DM 1000 LED microscope.

Immunofluorescence staining of the kidney was performed using an established procedure (Zhou et al., 2017). Briefly, the 4- μ m paraffin-embedded tissue sections were deparaffinized, rehydrated and incubated with the following primary antibodies at 4°C overnight: rabbit anti-cathepsin B (1:50, #PC41, Calbiochem), rabbit anti-cathepsin L (1:20, #168-10557, Raybiotech), rabbit anti-cathepsin S (from our own group; 1:100), rabbit anti-cathepsin K (1:50, #PB9856, Boster), rat anti-aquaporin-1 (1:50, #sc-9878, Santa Cruz Biotechnology), rat anti-ZO-1 (1:100, #sc-33725, Santa Cruz Biotechnology) and rat Alexa Fluor 594 anti-mouse E-cadherin (1:100, #147306, BioLegend, San Diego, CA), rabbit Alexa Fluor 594 anti-mouse cleaved caspase 3 (1:100, #8172, Cell Signaling Technology), followed by Alex Fluor 555 or 488-labelled secondary antibody detection. DAPI (#D9542, Sigma-Aldrich) was used to stain the nuclei. All images were collected by Olympus Fluoview FV1000 confocal laser scanning microscopy.

For cell immunofluorescent analysis, cells were seeded onto 8-well chamber slides. After stimulation with or without TGF- β (BD Bioscience, San Jose, CA), the slide was fixed in cold methanol and immunostained with rabbit anti-cathepsin B (1:50, #PC41, Calbiochem), rabbit anti-cathepsin L (1:20, #168-10557, Raybiotech), rabbit anti-cathepsin S (1:100) or rabbit anti-cathepsin K (1:50, #PB9856, Boster), mouse anti-fibronectin (1:100, #ab6328, Abcam), rabbit anti- α -SMA (1:750, #A2547, Sigma-Aldrich), rabbit anti-pSmad-2 (1:30, #3108S, Cell Signaling Technology) and rabbit anti-pSmad-3 (1:30, #9520S, Cell Signaling Technology), rabbit anti-importin β (1:100, #8673S, Cell Signaling Technology), RanBP3-FITC (1:100, #NBP2-42672F, Novus Biologicals, Littleton, CO), rat anti-TGFBR-1 (1:100, #MAB5871, R&D Systems, Minneapolis, MN), and rat anti-TGFBR2 (1:100, #MAB532, R&D Systems) antibodies, rat anti-aquaporin-1 (1:50, #sc-9878, Santa Cruz Biotechnology), and rat Alexa Fluor 594 anti-mouse E-cadherin (1:100, #147306, BioLegend), followed by Alex Fluor 555 or 488-labeled secondary antibody detection (Thermo Fisher Scientific). Sections were analyzed with a confocal microscopy for subcellular localization of Alex Fluor 555 or 488 (Olympus Fluoview FV1000; Olympus).

Western blot analysis, JPM labeling, and immunoprecipitation

For immunoblot analysis, an equal amount of proteins extracted from kidney cortex or primary cells were separated on SDS-PAGEs, blotted, and detected with different antibodies, including mouse anti- α -SMA (1:1000, #A2547, Sigma-Aldrich), rabbit anti-collagen-I (1:1000, #ab292, Abcam), rat anti-TGFBR1 (1:1000, #MAB5871, R&D Systems), rat anti-TGFBR2 (1:1000, #MAB532, R&D Systems), mouse anti-Imp- β monoclonal antibody (1:1000, #MA3-070, Thermo Fisher Scientific), mouse anti-RanBP3 monoclonal antibody (1:1000, #sc-373678, Santa Cruz Biotechnology), rabbit anti-pSmad-2 (1:1000, #3108S, Cell Signaling Technology), rabbit anti-Smad-2 (1:1000, #5339S, Cell Signaling Technology), rabbit anti-pSmad-3 (1:1000, #9520S, Cell Signaling Technology), rabbit anti-Smad-3 (1:1000, #9523S, Cell signaling Technology), rabbit anti-cathepsin B (1:1000, # PC41, Calbiochem), rabbit anti-cathepsin L (1:1000, #168-10557, Raybiotech), rabbit anti-cathepsin S (1:3000, was produced by our own group), rabbit anti-cathepsin K (1:1000, #PB9856, Boster), rabbit anti- β -Actin (1:1000, #4970S, Cell Signaling Technology) and rabbit anti-GAPDH (1:100, #2118S, Cell Signaling Technology) antibodies. Cytoplasm and nucleus from kidney epithelial cells were extracted according to the manufacturer's instructions (#78833, Thermo Fisher Scientific). β -Actin and fibrillarin (1:1000, #sc-166001, Santa Cruz Biotechnology) were used to reference protein in cytoplasm and nucleus, respectively.

JPM probe labeling was used to detect active cathepsins in kidney tissue extracts. Tissues or cells were lysed in a lysis buffer (pH 5.5) containing 1% Triton X-100, 40 mM sodium acetate, and 1 mM EDTA. Cathepsin active site JPM probe labeling was performed as described previously (Chen et al., 2013; Sun et al., 2012).

For immunoprecipitation, kidney epithelial cells were starved overnight in DMEM/F12 with 1% penicillin/streptomycin, followed by TGF- β stimulation for 24 h. Cells were lysed in an immunoprecipitation lysis buffer (0.025 M Tris, 0.15 M NaCl, 0.001 M EDTA, 1% NP-40, 5% glycerol; pH 7.4) and pre-cleared for 1 hour. Equal amounts of cell lysates (0.25 mg) were subsequently incubated overnight at 4°C with either antibody (goat anti-TGFBR1 antibody (10 μ g, #AF587, R&D Systems), goat anti-TGFBR2 antibody (10 μ g, # PA5-47719, Thermo Fisher Scientific), mouse anti-Imp- β monoclonal antibody (10 μ g, #MA3-070, Thermo Fisher Scientific), mouse anti-RanbP3 monoclonal antibody (10 μ g, #sc-373678, Santa Cruz Biotechnology) or IgG isotype control antibody (goat IgG isotype control antibody (10 μ g, #02-6202, Thermo Fisher Scientific) or mouse IgG isotype control antibody (10 μ g, #026502, Thermo Fisher Scientific)). The antibody-antigen complexes were captured, washed and eluted according to the manufacturer's instructions (#26149, Thermo Fisher Scientific). Immunoprecipitates were then resolved in SDS under reducing conditions, and followed by immunoblotting with rabbit anti-cathepsin B (1:1000, #PC41, Calbiochem), rabbit anti-cathepsin L (1:1000, #168-10557, Raybiotech), rabbit anti-cathepsin S (1:3000) or rabbit anti-cathepsin K (1:1000, #PB9856, Boster) antibodies to detect the immunocomplexes.

Isolation and culture of mouse kidney tubular epithelial cells

Primary tubular epithelial cells were prepared from renal cortical tissue from 8 to 10 weeks old male mice as previously described (Kimura et al., 2011). Briefly, mice were anesthetized and kidneys were harvested after cardiac perfusion with PBS. Kidney cortex was separated, minced and incubated with 1 mg/ml collagenase type II (#LS004177, Worthington Biochemical Corp., Lakewood, NJ) at 37 °C for 20 min, followed by 1 G sedimentation for 1 minute to discard pellet. Cells were centrifuged for 5 min at 1000 g and washed twice with PBS before plating. Cells were cultured in DMEM/F12 supplemented with 10% FBS and 10 ng/ml murine EGF (#SRP3196, Sigma-Aldrich) and plated on 0.2% matrigel (1:500 diluted in PBS, #CB 40234, Thermo Fisher Scientific) coated plates. After starved with DMEM/F 12 with 1% penicillin/streptomycin overnight, cells were stimulated with or without 2 ng/ml TGF- β in serum free medium for the indicated time and lysed for western blot, immunoprecipitation, or fixed for immunofluorescent staining.

Flow cytometry

Primary kidney TECs were resuspended in PBS, and incubated with cell-surface marker PE anti-mouse E-cadherin antibody (1.0 μ g per million cells in 100 μ l, #147304, BioLegend) or isotype control for 30 min on ice, following separated by using a flow cytometer BD FACSCanto™ II (BD Biosciences). Data were analyzed using FlowJo V10.

Statistical analysis

All data were presented as means \pm SEM. Because of relatively small sample sizes and often skewed data distribution, we selected the non-parametric Mann-Whitney *U* test for paired data sets and one-way ANOVA with post-hoc Bonferroni test was used for comparison among three or more groups to examine statistical significance. *P*<0.05 was considered as statistically significant.

REFERENCES

- Chen, H., Wang, J., Xiang, M.X., Lin, Y., He, A., Jin, C.N., Guan, J., Sukhova, G.K., Libby, P., Wang, J.A., *et al.* (2013). Cathepsin S-mediated fibroblast trans-differentiation contributes to left ventricular remodelling after myocardial infarction. *Cardiovasc Res* 100, 84-94.
- Kimura, T., Takabatake, Y., Takahashi, A., Kaimori, J.Y., Matsui, I., Namba, T., Kitamura, H., Niimura, F., Matsusaka, T., Soga, T., *et al.* (2011). Autophagy protects the proximal tubule from degeneration and acute ischemic injury. *J Am Soc Nephrol* 22, 902-913.
- Sun, J., Sukhova, G.K., Zhang, J., Chen, H., Sjoberg, S., Libby, P., Xia, M., Xiong, N., Gelb, B.D., and Shi, G.P. (2012). Cathepsin K deficiency reduces elastase perfusion-induced abdominal aortic aneurysms in mice. *Arterioscler Thromb Vasc Biol* 32, 15-23.
- Zhou, Y., Chen, H., Liu, L., Yu, X., Sukhova, G.K., Yang, M., Zhang, L., Kytтарis, V.C., Tsokos, G.C., Stillman, I.E., *et al.* (2017). CD74 Deficiency Mitigates Systemic Lupus Erythematosus-like Autoimmunity and Pathological Findings in Mice. *J Immunol* 198, 2568-2577.

SUPPLEMENTAL FIGURES

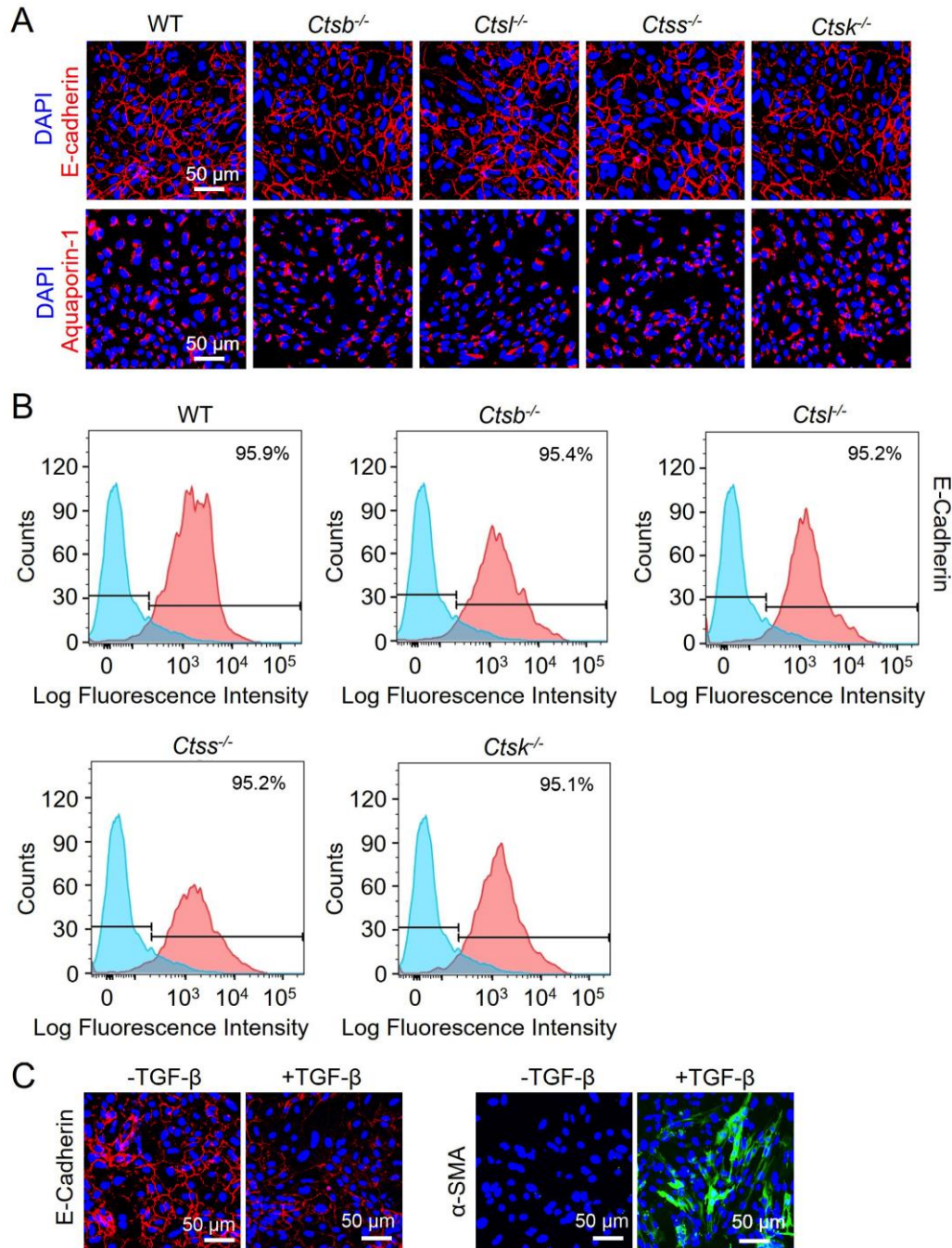


Figure S1. Characterization of renal cortical TECs isolated from wild-type, related to Figure 1. *Ctsb*^{-/-}, *Ctstl*^{-/-}, *Ctss*^{-/-} and *Ctsk*^{-/-} mice. **(A)** Immunofluorescent staining detected the expression of E-cadherin (red) or aquaporin-1 (red) with nuclei counterstained with DAPI (blue). **(B)** FACS analysis of TECs after staining with E-cadherin-PE antibody (red histogram) or rat IgG isotype control (blue histogram). **(C)** Immunofluorescent staining detected the expression of E-cadherin (red) or α -SMA (green) with nuclei counterstained with DAPI (blue) in WT mouse TECs treated without and with TGF- β (2 ng/mL, 24 hrs). Scale bar: 50 μ m.

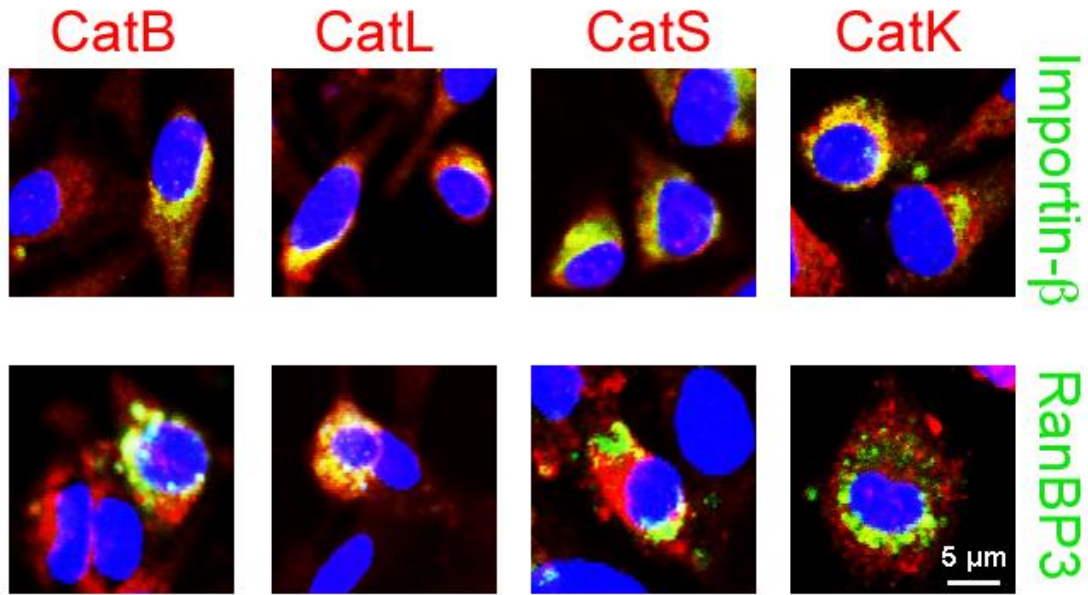


Figure S2. Cathepsin colocalization with importin- β and RanBP3 in mouse kidney TECs, related to Figure 3. Immunofluorescent double staining of different cathepsins (red) and importin- β (green) or RanBP3 (green), with nuclei counterstained with DAPI (blue) in TECs from WT mice. Scale bar: 5 μ m.

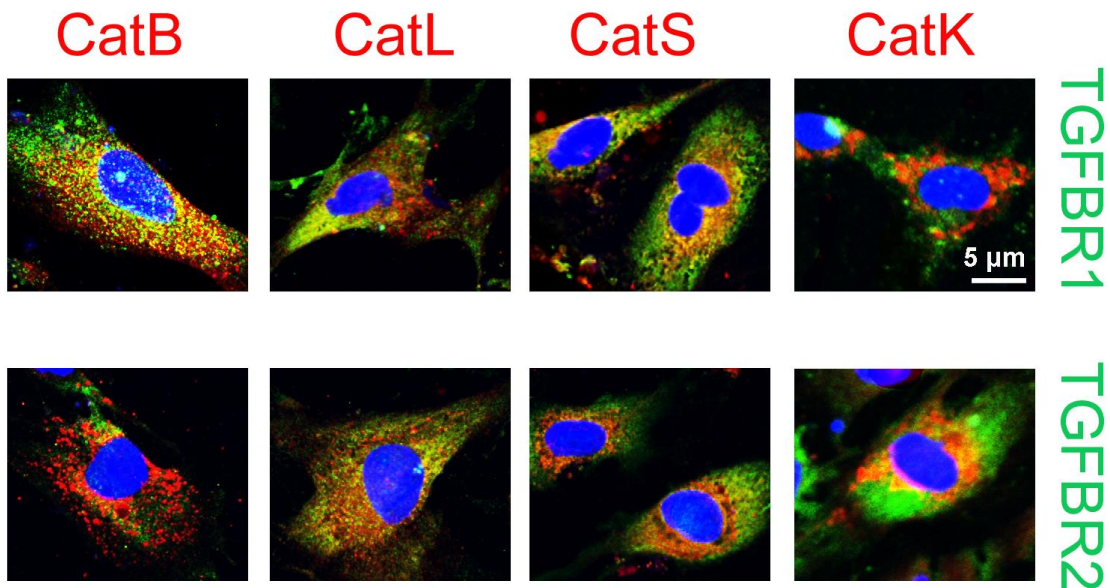


Figure S3. Cathepsin colocalization with TGF- β receptor 1 (TGFBR1) and TGF- β receptor 2 (TGFBR2) in mouse kidney TECs, related to Figure 4. Immunofluorescent double staining of different cathepsins (red) and TGFBR1 (green) or TGFBR2 (green), with nuclei counterstained with DAPI (blue) in TECs from WT mice. Scale bar: 5 μ m.

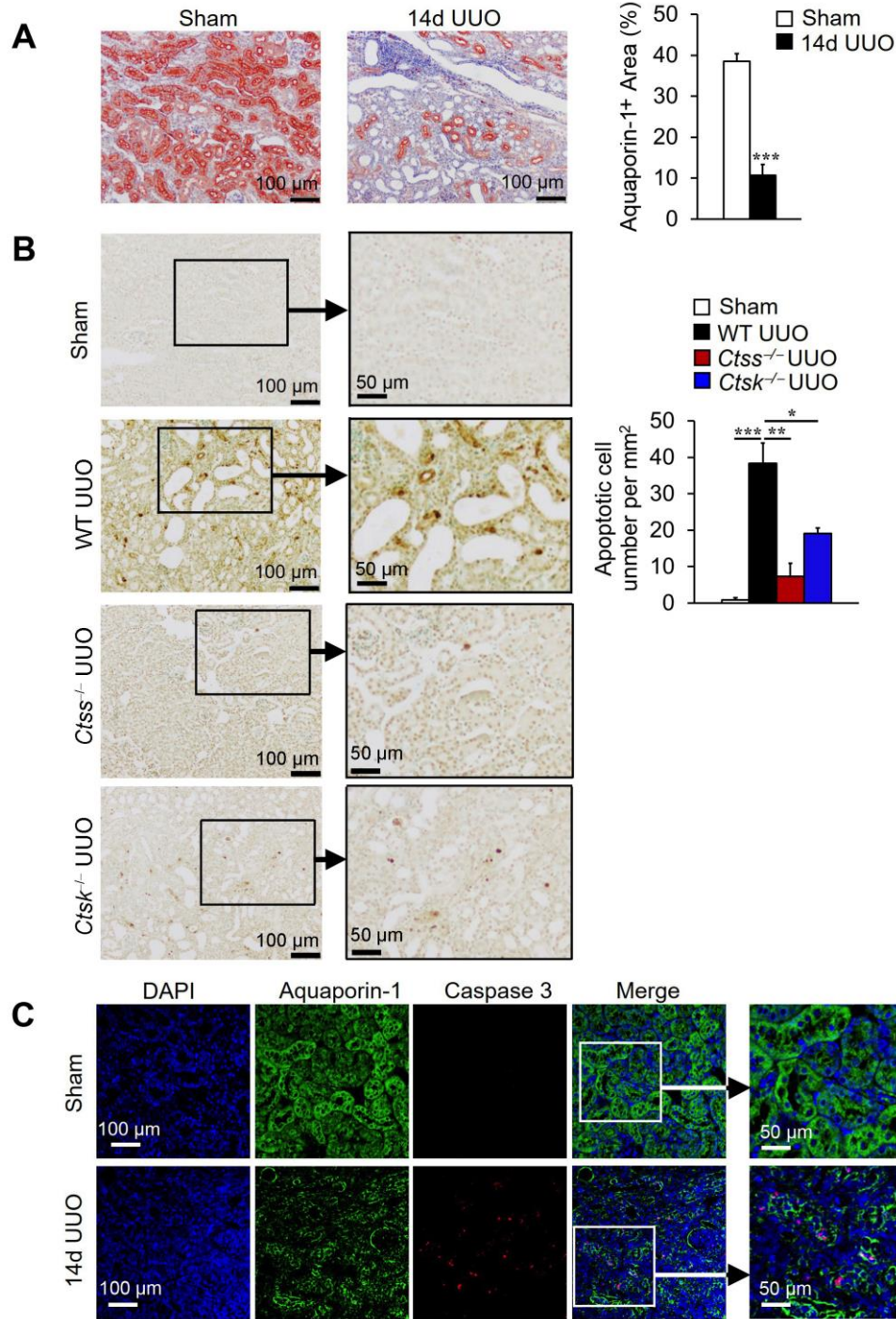


Figure S4. Kidney cortical proximal tubular damage at 14 days after UUU in wild-type mice, related to Figure 5. Immunostaining detected E-cadherin-positive area (**A**) and TUNEL-positive apoptotic cell numbers (**B**) in kidney sections from sham and UUU-injured mice as indicated. Representative images are shown to the left. (**C**) Immunofluorescent double staining of proximal tubular marker aquaporin-1 (green) and cleaved caspase 3 (red), with nuclei counterstained with DAPI (blue) in kidney section from sham and 14 days post-UUU mice as indicated. Scale: 100 μm ; Inset scale: 50 μm . $n=8\sim 10$ per group. * $p<0.05$, ** $p<0.01$, *** $p<0.001$.

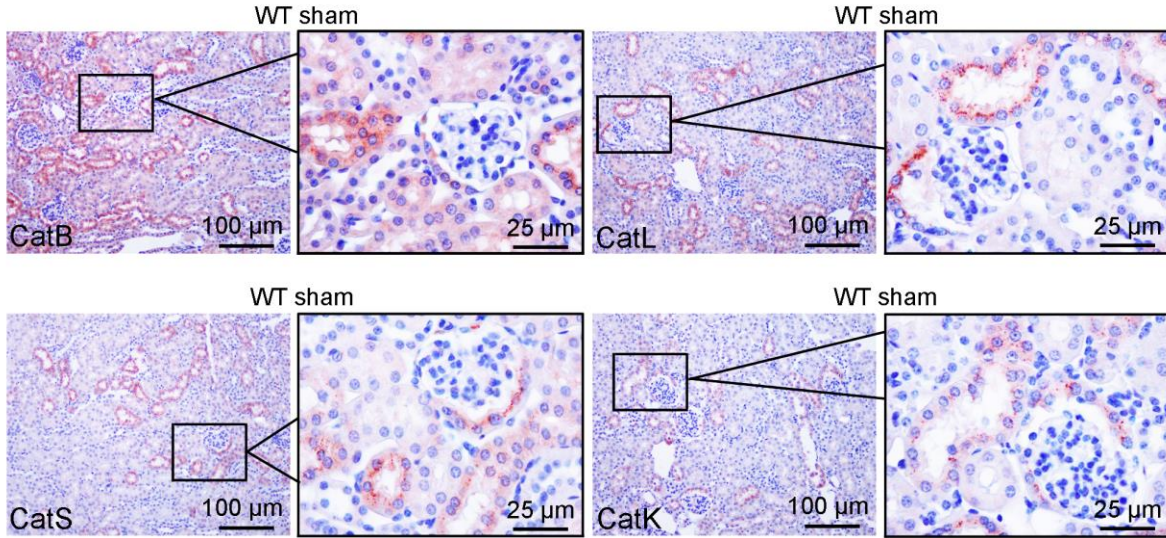


Figure S5. Immunostaining detected cathepsin expression in the tubular epithelial cells from normal mouse kidneys, related to Figure 5. No cathepsin expression was detected in the glomeruli. n=8~10 per group. Scale bar: 100 μm , inset scale: 25 μm .

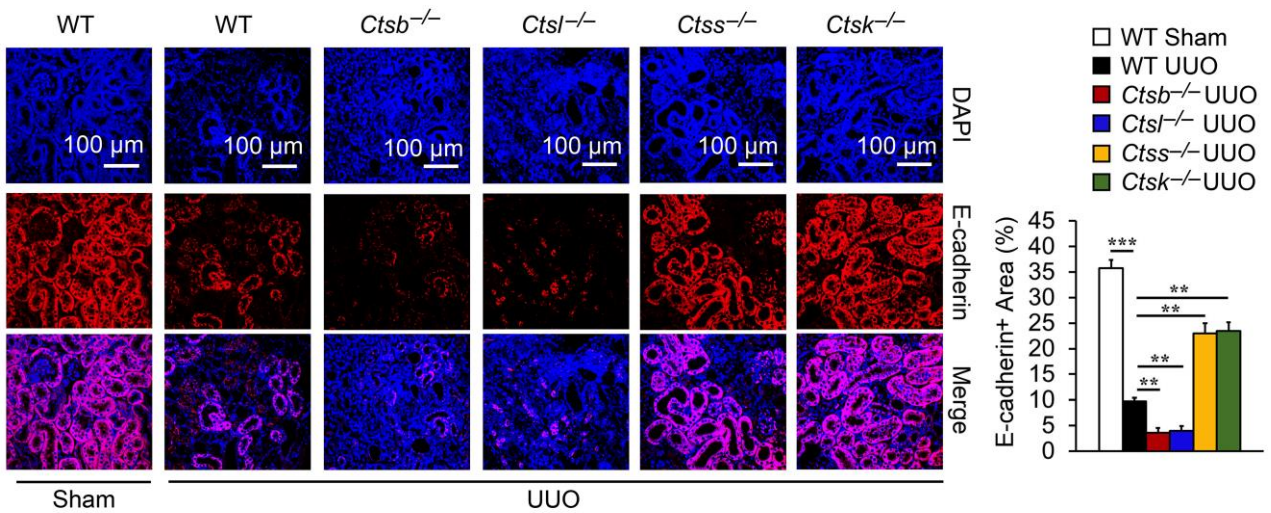


Figure S6. Immunofluorescent staining detected epithelial cell marker E-cadherin (red), with nuclei counterstained with DAPI (blue) in kidney section from different post-UUO mice as indicated, related to Figure 7. Scale bar: 100 μm . n=8~10 per group. * p <0.05, ** p <0.01, *** p <0.001. Representative images are shown to the left.